NUREG/CR-1506
BNL-NUREG-51218
AN, R-1,4,5

WATER REACTOR SAFETY RESEARCH DIVISION

QUARTERLY PROGRESS REPORT
JANUARY 1 - MARCH 31, 1980

HERBERT J.C. KOUTS, Departmen. Chairman
WALTER Y. KATO, Deputy Chairman

Principal Investigators:

N. Abuaf
M.M. Levine
P. Saha
D. van Rooyen

Compiled by: Anthony J. Romano
Manuscript Completed: May 1980

DEPARTMENT OF NUCLEAR ENERGY
BROOKHAVEN NATIONAL LABORATORY, ASSOCIATED UNIVERSITIES, INC.
UPTON, NEW YORK 11973

Prepared for the
REACTOR SAFETY RESEARCH DIVISION
OFFICE OF NUCLEAR REGULATORY RESEARCH
U.S. NUCLEAR REGULATORY COMMISSION
Contract No. DE-AC02-76CH00016
FIN Nos.:

A-3014
A-3045
A-3208
A-3215

NOTICE

Available from
GPO Sales Program
Division of Technical Information and Document Control
U.S. Nuclear Regulatory Commission
Washington, D.C. 20555
and
National Technical Information Service
Springfield, Virginia 22161

FOREWORD

The Water Reactor Safety Research Programs Quarterly Report describes current activities and technical progress in the programs at Brookhaven National Laboratory sponsored by the USNRC Division of Reactor Safety Research. The projects reported each quarter are the following: LWR Thermal Hydraulic Development, Advanced Code Evaluation, TRAC Code Assessment, and Stress Corrosion Cracking of PWR Steam Generator Tubing.

The previous reports, BNL-NUREG-50624, BNL-NUREG-50661, BNL-NUREG-50683 BNL-NUREG-50747, BNL-NUREG-50785, BNL-NUREG-50820, BNL-NUREG-50883, BNL-NUREG-50931, BNL-NUREG-50978, BNL-NUREG-51015, BNL-NUREG-51081, BNL-NUREG-51131, and BNL-NUREG-51178 have covered the periods October 1, 1976 through December 31, 1979.

WATER REACTOR SAFETY RESEARCH

TABLE OF CONTENTS

I. LIGHT WATER REACTOR SAFETY

SUMMARY

During this quarter, a preliminary data evaluation report (BNL-NUREG-27138) and a short technical memo comparing the Alamgir-Lienhard inception correlation prediction with the Marviken large vessel data, were submitted to NRC. In addition, a report on critical flashing flows (BNL-NUREG-27512) was transmitted to NRC, summarizing the application of the Alamgir-Lienhard correlation to flowing systems and the resulting prediction of critical flow rates in nozzles with subcooled inlet conditions.

Recent BNL flashing experiment data which include the axial pressure distribution and the axial area-averaged void fraction distributions have been evaluated. The vapor generation rates Γ_v in these experiments have been computed from the pressure and void data and a drift model (V_{gj}). The possible errors in the V_{gj} model have been shown to lead to insignificant uncertainties in Γ_v, based on measurements (Thang and Davis, 1969) in air-water flows in a converging-diverging nozzle. The sensitivity of the Γ_v values on the distribution parameter C_o could be of the order of ± 30% and higher for large α's ($\alpha > 0.6$). Comparison with the vapor generation rates assumed in TRAC-P1A code showed that TRAC overestimates the vapor generation rate in low mass flux experiments which exhibited a greater departure from equilibrium. When flashing occurred close to equilibrium, TRAC's calculation of Γ_v was closer to the values derived from the experimental data.

After repairing and replacing two major components of the water loop test facility which had failed earlier, all the pressure transducers, thermocouples and the γ-densitometer were recalibrated.

RAMONA-III code assessment activities highlighted the need to change certain aspects of the hydraulics modelling and cross section parameterization. A different slip correlation was incorporated and previously neglected compressibility terms were added to the equation for volumetric flow. A new cross section formalism was requested for the future, and in the interim calculations were done with neutronics data used in two-dimensional studies of the Peach Bottom-2 Turbine Trip Tests. Results with RAMONA-III for the initial axial power distribution and the time dependence of power for all three tests were in good agreement with the measured data. Calculations of heated channel experiments also helped confirm the validity of the code.

The Mark II version of the IRT once-through steam generator model has been run on a stand alone basis and the results are in reasonably good agreement with the Mark I version. The new model is currently being implemented in the IRT code.

RETRAN code input decks for the Sequoyah reactor have been obtained from the Tennessee Valley Authority. These input decks are currently being modified for use on the BNL CDC-6600.

Work on the independent assessment of TRAC-P1A has continued with the various one-dimensional steady-state and transient experiments, as well as the RPI phase separation tests and the FRIGG loop tests.

All of the NRC-specified tests of the Moby-Dick nitrogen-water and the KFK-IRE nozzle flow experiments have been simulated with TRAC-P1A. The sensitivity of the TRAC predictions to the two-phase friction factors has been assessed through these simulations. The assessment effort with the University of Houston flooding tests has begun, and the region where TRAC-P1A will not be applicable has been pointed out.

Several tests of the Super-CANON and the Marviken experiments have been simulated by TRAC-P1A during the reporting quarter, and the results have been discussed in detail. Assessment with the Battelle-Frankfurt top blowdown tests has also begun.

Simulation of the RPI phase separation tests now includes runs with rods. However, even with the rods, the code does not reach a true steady-state. For one test with rods and one outlet, the code seemed to reach near a steady-state. The FRIGG test was tried with the one-dimensional option of the vessel module. However, the code again failed to reach a steady-state. But, the simulation of the same test with the one-dimensional pipe component was successful.

Finally, the Alamgir-Lienhard correlation for nucleation delay is being implemented in the BNL version of TRAC-P1A.

1. Light Water Reactor Thermal/Hydraulic Development Program

1.1 Analytical Modeling (B.J.C. Wu and N. Abuaf)

1.1.1 Determination of Vapor Generation Rate from Experimental Data.

The net vapor generation rate Γ_v in flashing flows may be expressed as a function of the gradients of the cross-sectional area-averaged void fraction α, the local static pressure p, and the local mass flux G (Zimmer et al. 1979):

$$\Gamma_v = \frac{\frac{Gx}{\alpha}\frac{d\alpha}{dz} + \frac{Gx}{\rho_g}(1-\alpha C_o)\frac{d\rho_g}{dp}\cdot\frac{dp}{dz} - \frac{\alpha\rho_g V_{gj}}{G}\cdot\frac{dG}{dz}}{1 - \alpha C_o (\rho_f - \rho_g)/\rho_f} \tag{1.1}$$

where z is the axial coordinate in the flow direction, x is the quality, ρ_f and ρ_g are the liquid and vapor densities, respectively, C_o is the distribution parameter and V_{gj} is the vapor drift velocity which is assumed to be given by

$$V_{gj} = K\left[\frac{\sigma g (\rho_f - \rho_g)}{\rho_f^2}\right]^{1/4} \tag{1.2}$$

where the coefficient K = 1.41 according to Kroeger and Zuber (1968).

By using the experimentally measured values of the α and p distributions and the nozzle mass flow rate together with a hydrodynamic calibration of the nozzle, one may evaluate each term in Eq. (1.1) and determine Γ_v provided C_o and V_{gj} are known.

It has been shown previously (Zimmer et al. 1979) that a variation of K in Eq. (1.2) from 0 (no slip) to 14.1 (a ten-fold increase) produced only an insignificant change in the Γ_v value calculated from Eq. (1.1) because the term involving V_{gj} in Eq. (1.1) contributes only about 1% to Γ_v. Thus, this method of determining Γ_v is insensitive to larger uncertainties in V_{gj} (unless orders-of-magnitude variations are expected).

Recently Thang and Davis (1979) have measured the diametrical distribution of void fraction and slip in air-water two-phase flows in a converging-diverging nozzle. Based on the geometry of their nozzle, fluid acceleration and deceleration in Thang and Davis' experiments are estimated to be greater than those in the BNL experiments by a factor of two to four. Their measurements indicated that V_{gj} increased from 0.58 m/s to about 0.83 m/s for α = 0.3 to α = 0.5. Using Eq. (1.2) V_{gj} is found to be about 0.23 m/s. The sensitivity calculations covering a range for V_{gj} of 0 to 2.3 m/s show that the possible error in V_{gj} being within one order of magnitude, it is not expected to affect the Γ_v calculation appreciably.

The latest BNL experimental results with pressure distribution and transverse and axial distributions of chordal averaged void fraction measurements have been evaluated to obtain Γ_v data using Eq. (1.1) and (1.2). The results of the calculations using data from one series of experiments at T_{in} =

121 C are shown in Figures (1.1) to (1.4). These data are presented in order of increasing mass flow rate, or increasing vapor production rate. Plots A and B in each of the Figures (1.1) to (1.4), compare the measured pressure and area-averaged void fraction distributions (the square symbols) with the least-square cubic-spline fits (continuous curves) to the data. The "plus-sign" symbols in these plots are the location of the optimum knots where adjacent pieces of cubic splines are joined together maintaining continuity up to the second derivative.* Plots C through G in each of the figures depict the vapor generation rates calculated from the derivatives of the cubic spline fits in A and B, using the value of the distribution parameter shown. It is seen that varying the distribution parameter in the range $0.8 \leq C_o \leq 1.2$ leads to a $\pm$ 30% change in Γ_v except at very high void fractions ($\alpha > 60\%$). Comparison with TRAC-P1A (see following section) predictions indicated large discrepancies in Γ_v at low mass fluxes, and fair agreement was found at higher mass fluxes.

1.1.2 Comparison with Computer Codes (TRAC-P1A)

The experimental data (pressure profiles and area averaged void distributions) are being compared with TRAC-P1A predictions. Table 1.1 presents the inlet pressures and comparison of the experimentally measured mass flow rates with TRAC predictions for the 121 C inlet temperature runs.

The top figure in Figure 1.5 shows a comparison of the experimental pressure distributions and area-averaged void profiles with TRAC-P1A predictions. Since the TRAC inception criterion for vapor generation is at the location where the local liquid temperature corresponding to the local pressure is equal to the saturation temperature, voids in TRAC tend to be generated upstream of the throat. In contrast, the experimental area-averaged void profile shows the existence of single phase flow in the whole test section. In the bottom figure (Fig. 1.5) we compare the vapor generation rates ($\Gamma_v = G\ dx/dz$) calculated from the TRAC-P1A listed cell properties and flow parameters (Wu 1979), with those calculated from the experimental data ($C_o = 1.0$) using Eq. (1.1) and the cubic spline fit described in Section 1.1.1. Increasing C_o to 1.2 does not change the dotted line presented in Fig. 1.5.

Figs. 1.6 and 1.7 depict similar results wherein the vapor generation rates calculated from TRAC-P1A cell properties are compared with the vapor generation rates calculated from the experimentally measured pressure profiles and area averaged void distributions which were presented in the October-December 1979 Quarterly (Figs. 1.7 and 1.8). Finally, in Fig. 1.8, similar comparisons as those presented above for the higher mass flow rate experiments (11.9 Kg/s) at 121 C inlet temperature are observed. Once again the top figure compares the experimental pressure and area averaged void profiles with TRAC-P1A calculations. In the bottom figure, the experimentally derived vapor generation rates are compared with the values obtained from hand calculations based on the TRAC-P1A listed properties (solid line), as well as with the direct printout of the vapor generation rates calculated internally by TRAC (circles) (Saha and

* The apparent discontinuity in slope in some of the curves is because of the finite number of points plotted. The "curves" are actually series of straight lines connecting neighboring points plotted.

Sanborn, 1980). The Γ_v values calculated from the cell properties appear to be very close and almost identical to those taken directly from TRAC. The TRAC calculations for Run 137 did not cvonverge to a steady state solution when the homogeneous flow friction factor option was used. The results presented were obtained with the use of the annular flow friction factor option. (Saha and Sanborn 1980).

Although the effect of V_{gj} on the calculated Γ_v's is negligible, the effect of the distribution parameter C_o, is still observed to persist and is important at high void fractions.

In summary, comparisons of TRAC-P1A calculations with vapor generation rates derived from experimental measurements lead to the following conclusions: In the low-mass-flux Run 141/142, peak Γ_v predicted by TRAC was more than one order of magnitude higher than the "experimental" value shown in Fig. (1.1). The TRAC prediction for Run 145/146 at intermediate mass flux was about twice as high as in Fig. (1.2), while for the high mass flux Runs 133/134 and 140/139 the TRAC calculations roughly agreed with the experimentally derived values of Γ_v assuming C_o = 1.1. The origin of this discrepancy may be partly attributed to TRAC's inability to predict the flashing inception point.

1.2 Flashing Experiments (G.A. Zimmer, J.H. Klein, B.J.C. Wu, N. Abuaf)

In December 1979, while restarting the water loop to finish the last series of runs to fulfill the test matrix, one of the 8-inch diameter, schedule 40 pipe sections which houses two 100 kw heater bundles was found to be cracked and leaking. This was the same heater which was burned out during the last series of runs and the failure was attributed to localized heating or to electrical arcing during the failure. The damaged heater shell was removed from the loop, a new assembly was built at the BNL machine shop and replaced in the loop.

During the calibration of the loop instrumentation, the old multichannel scanner which was obtained from Government surplus and which is the basis of the automatic data acquisition system broke down. The scanner was replaced with a new one which was purchased for such an emergency, and the wiring of all the sensors to the new scanner was accomplished.

Using the new scanner, calibration of all pressure transducers and thermocouples in the loop were performed as well as the empty (air) and full calibrations of the test section for the gamma densitometry.

REFERENCES

KROEGER, P. G., and Zuber, N., "An Analysis of the Effects of Various Parameters in the Average Void Fractions in Subcooled Boiling," Int. J. Heat Mass Transfer 11, 211, 1968.

SAHA, P., and Sanborn, Y., Personal Communication, 1980.

THANG, N. T. and Davis, M. R., "The Structure of Bubbly Flow Through Venturis," Int. J. Multiphase Flow, 5, pp 17-37, 1979.

WU, B. J. C., "Water Reactor Safety Research Division, Quarterly Progress Report, April-June 1979," BNL-NUREG-51081, p. 6, 1979.

ZIMMER, G. A., Wu, B. J. C., Leonhardt, W. J., Abuaf, N., and Jones, O. C., Jr., "Pressure Distribution in a Converging-Diverging Nozzle with Nonequilibrium Water Vapor Generation," BNL-NUREG-26003, 1979.

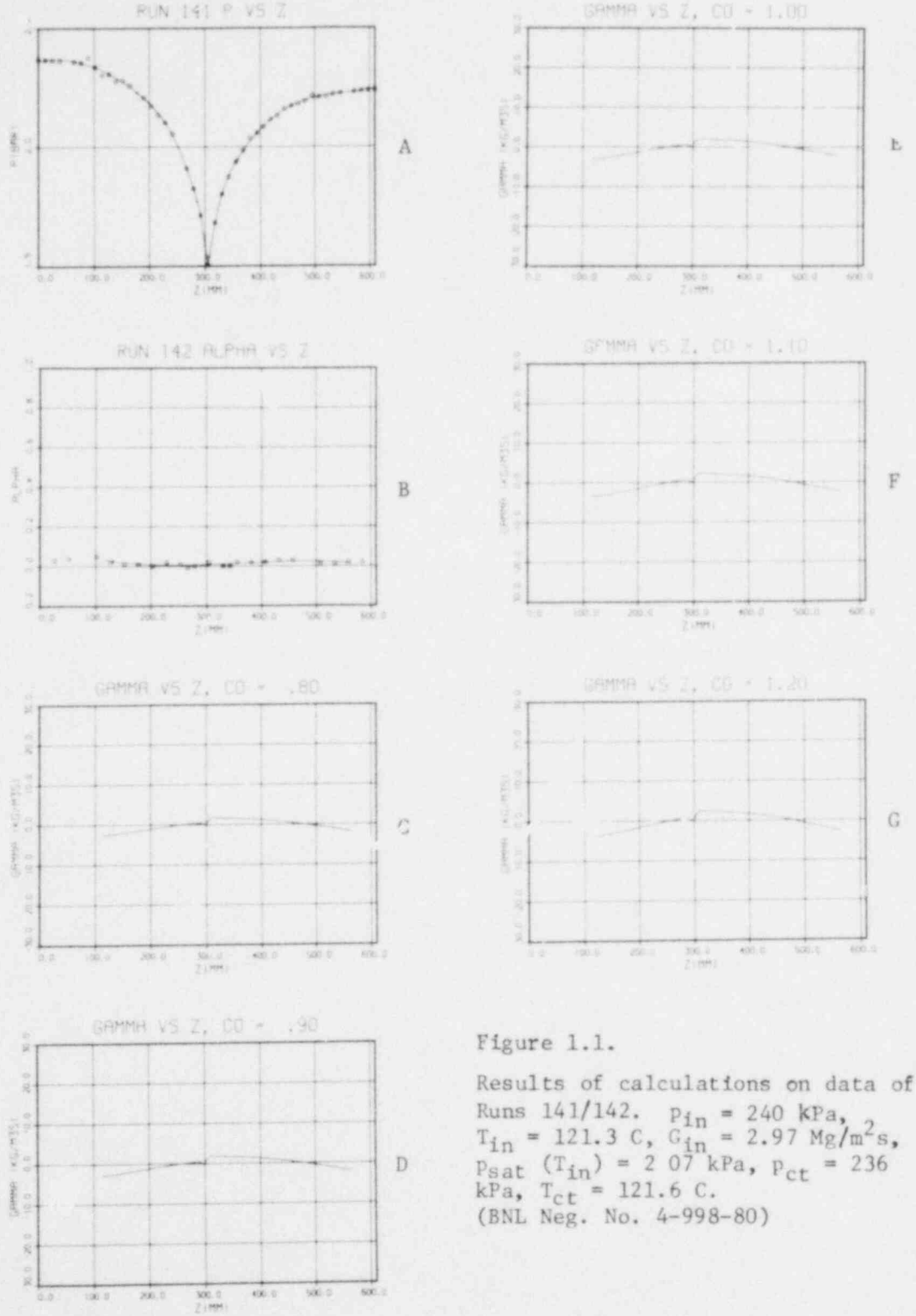

Figure 1.1.

Results of calculations on data of Runs 141/142. p_{in} = 240 kPa, T_{in} = 121.3 C, G_{in} = 2.97 Mg/m^{2}s, P_{sat} (T_{in}) = 2 07 kPa, p_{ct} = 236 kPa, T_{ct} = 121.6 C.
(BNL Neg. No. 4-998-80)

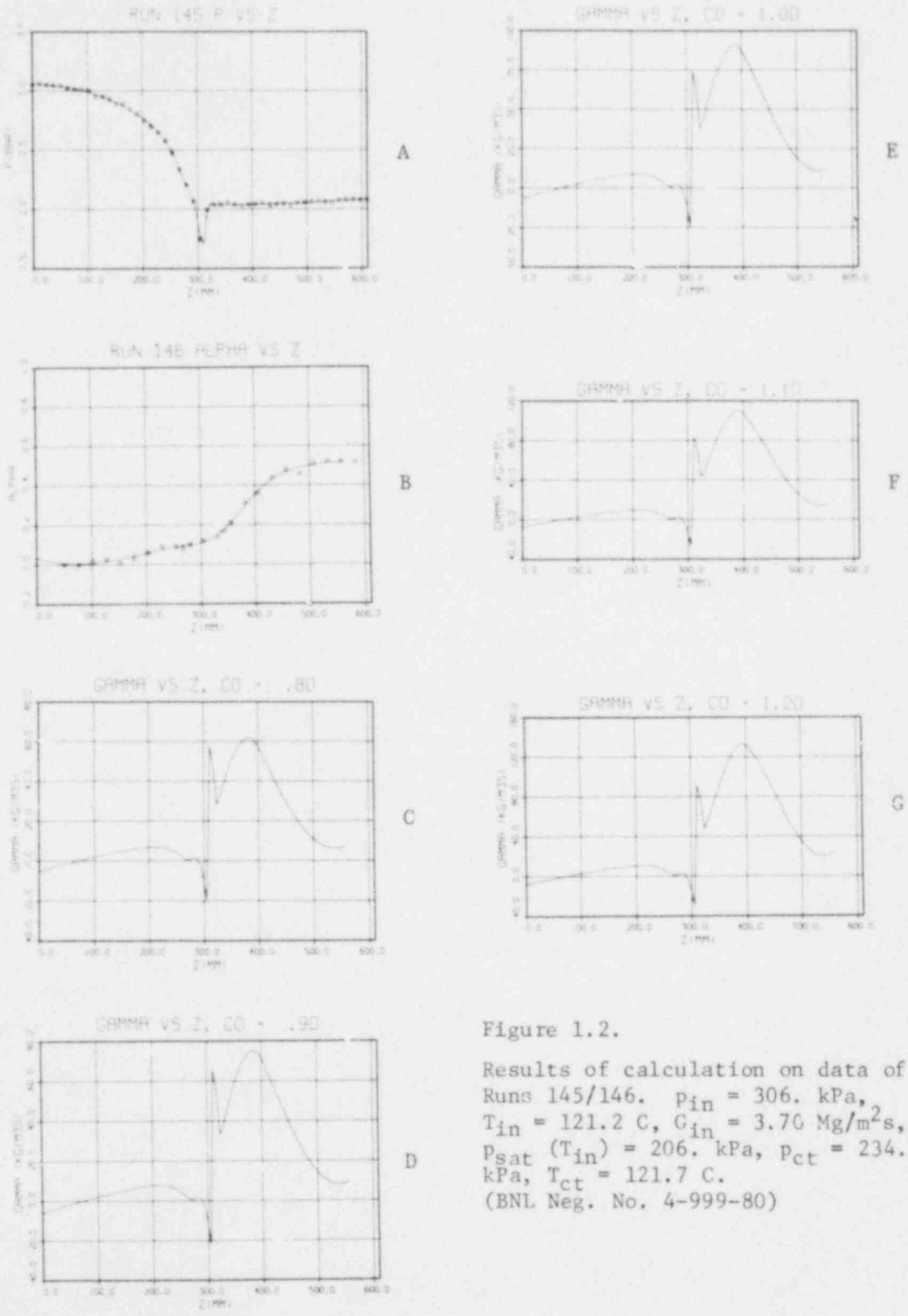

Figure 1.2.

Results of calculation on data of Runs 145/146. p_{in} = 306. kPa, T_{in} = 121.2 C, G_{in} = 3.70 Mg/m^2s, p_{sat} (T_{in}) = 206. kPa, p_{ct} = 234. kPa, T_{ct} = 121.7 C.
(BNL Neg. No. 4-999-80)

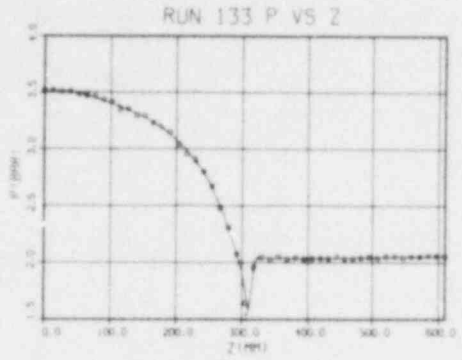

A

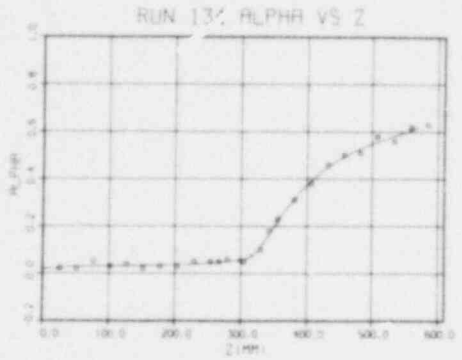

B

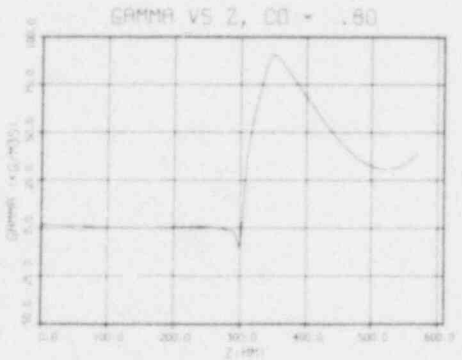

C

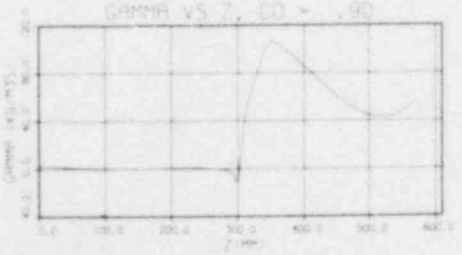

D

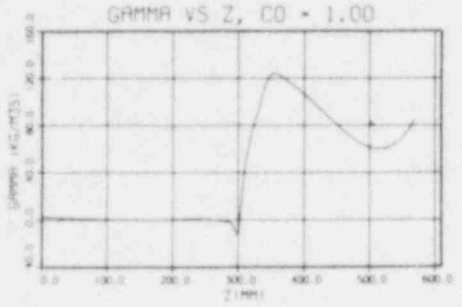

E

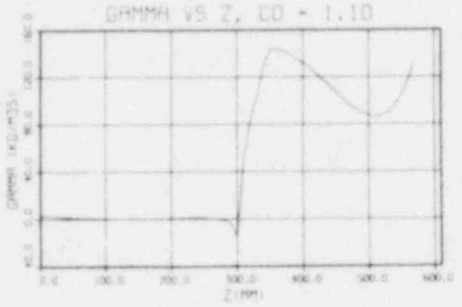

F

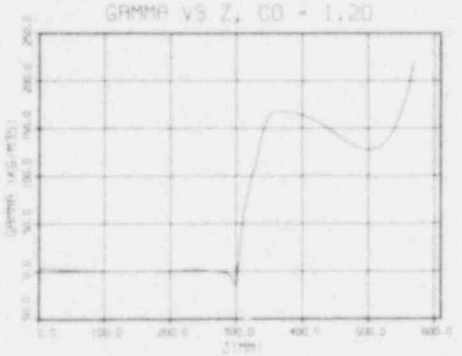

G

Figure 1.3.

Results of calculations on data of Runs 133/134. p_{in} = 350 kPa, T_{in} = 121.2 C, G_{in} = 4.43 Mg/m^{2}s, P_{sat} (T_{in}) = 206. kPa, p_{ct} = 233. kPa, T_{ct} = 121.7 C.
(BNL Neg. No. 4-937-80)

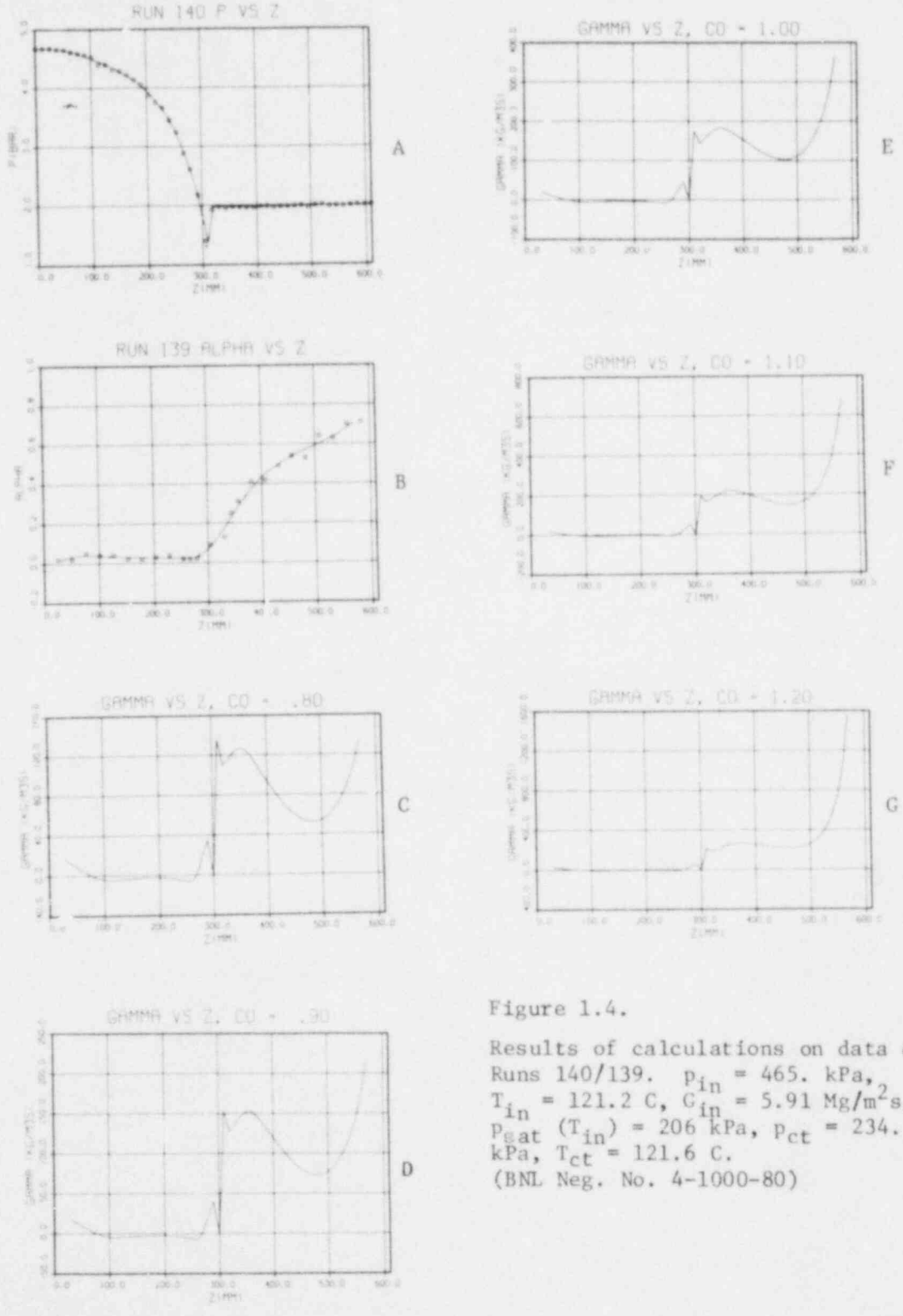

Figure 1.4.

Results of calculations on data of Runs 140/139. p_{in} = 465. kPa, T_{in} = 121.2 C, G_{in} = 5.91 Mg/m^{2}s, p_{sat} (T_{in}) = 206 kPa, p_{ct} = 234. kPa, T_{ct} = 121.6 C.
(BNL Neg. No. 4-1000-80)

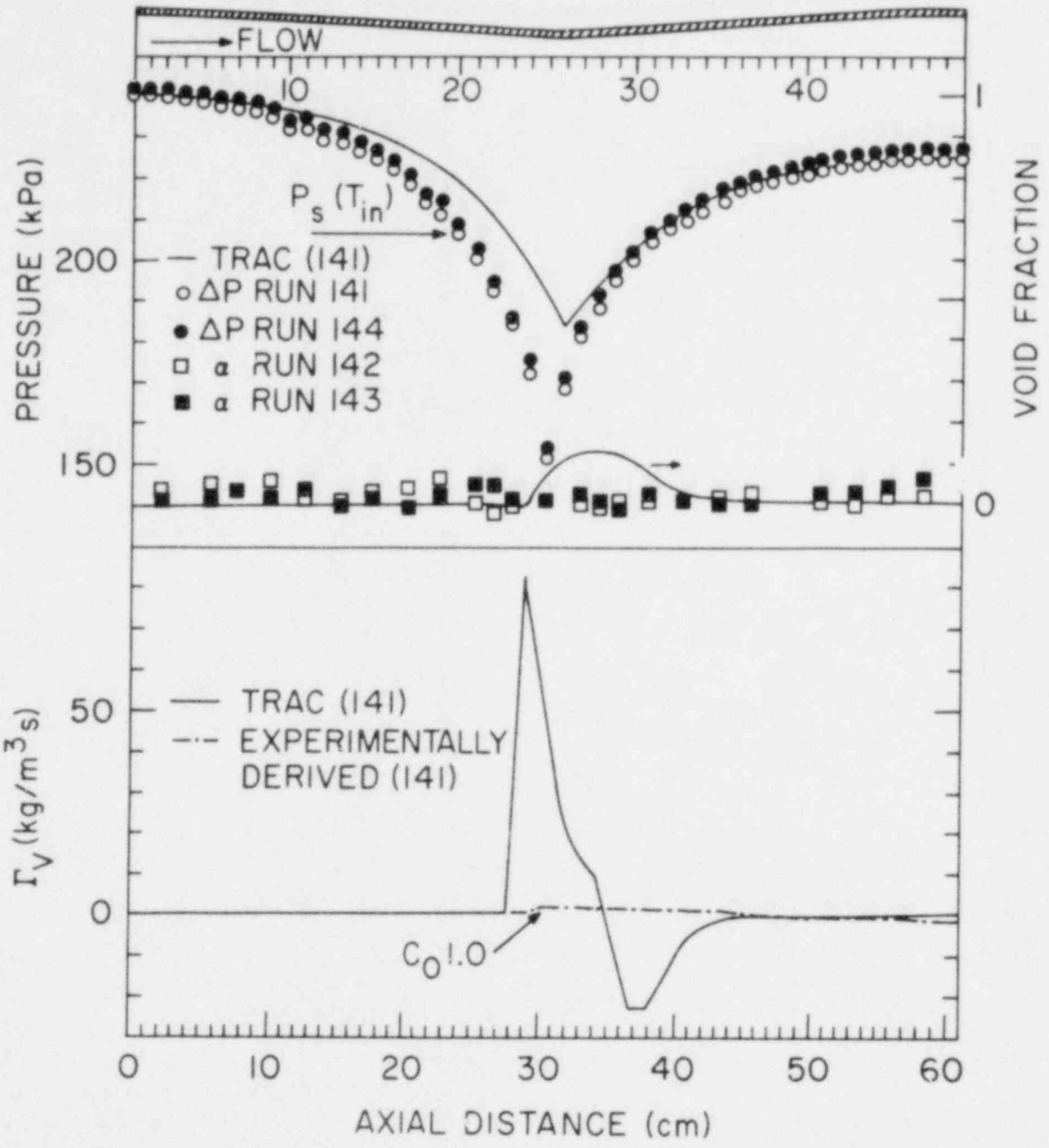

Figure 1.5. Comparison of experimentally measured pressure distributions and area averaged void profiles, as well as vapor generation rates calculated from the experimental data with TRAC-P1A predictions. (BNL Neg. No. 5-276-80)

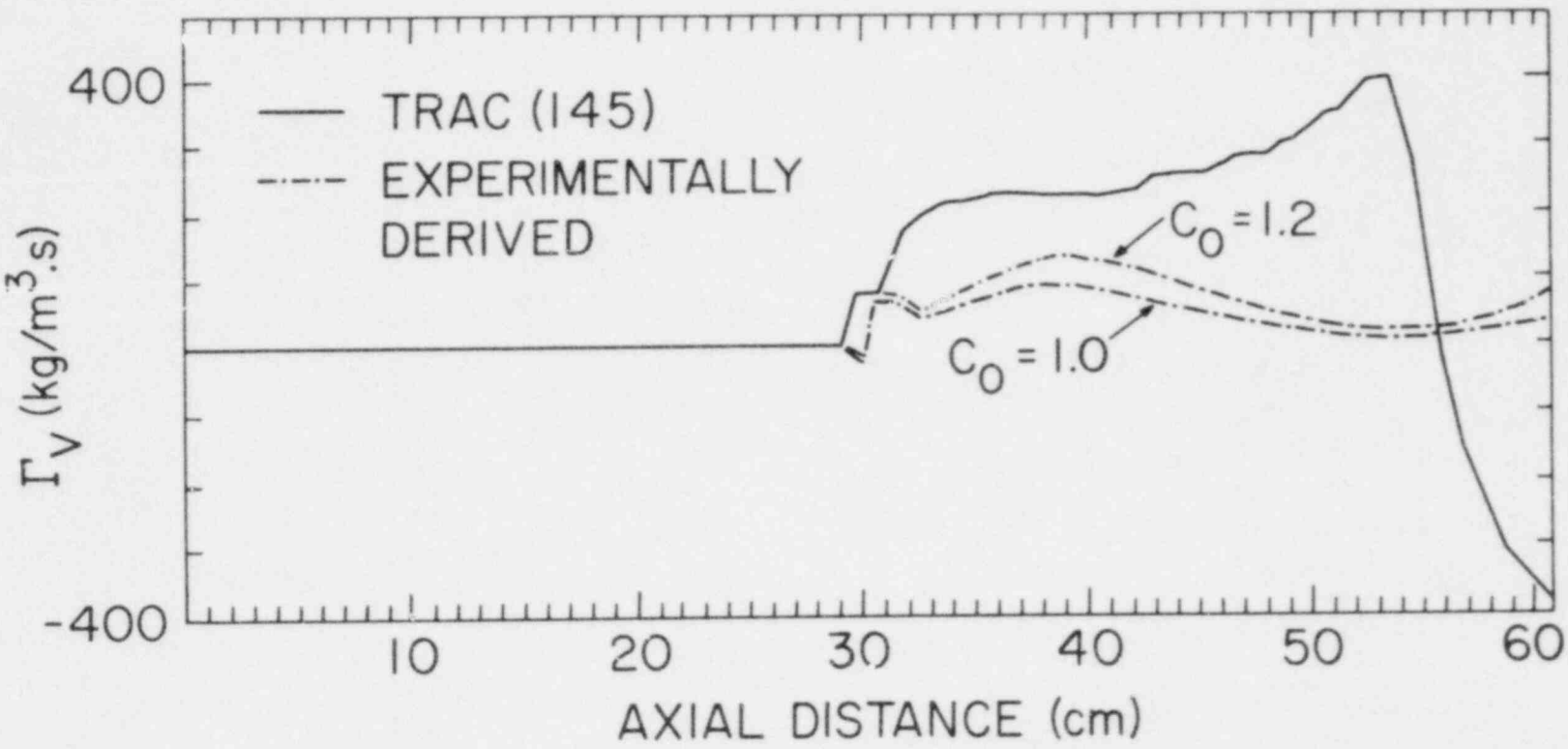

Figure 1.6. Comparison of vapor generation rates calculated from experimental data with TRAC-P1A predictions. (BNL Neg. No. 5-277-80)

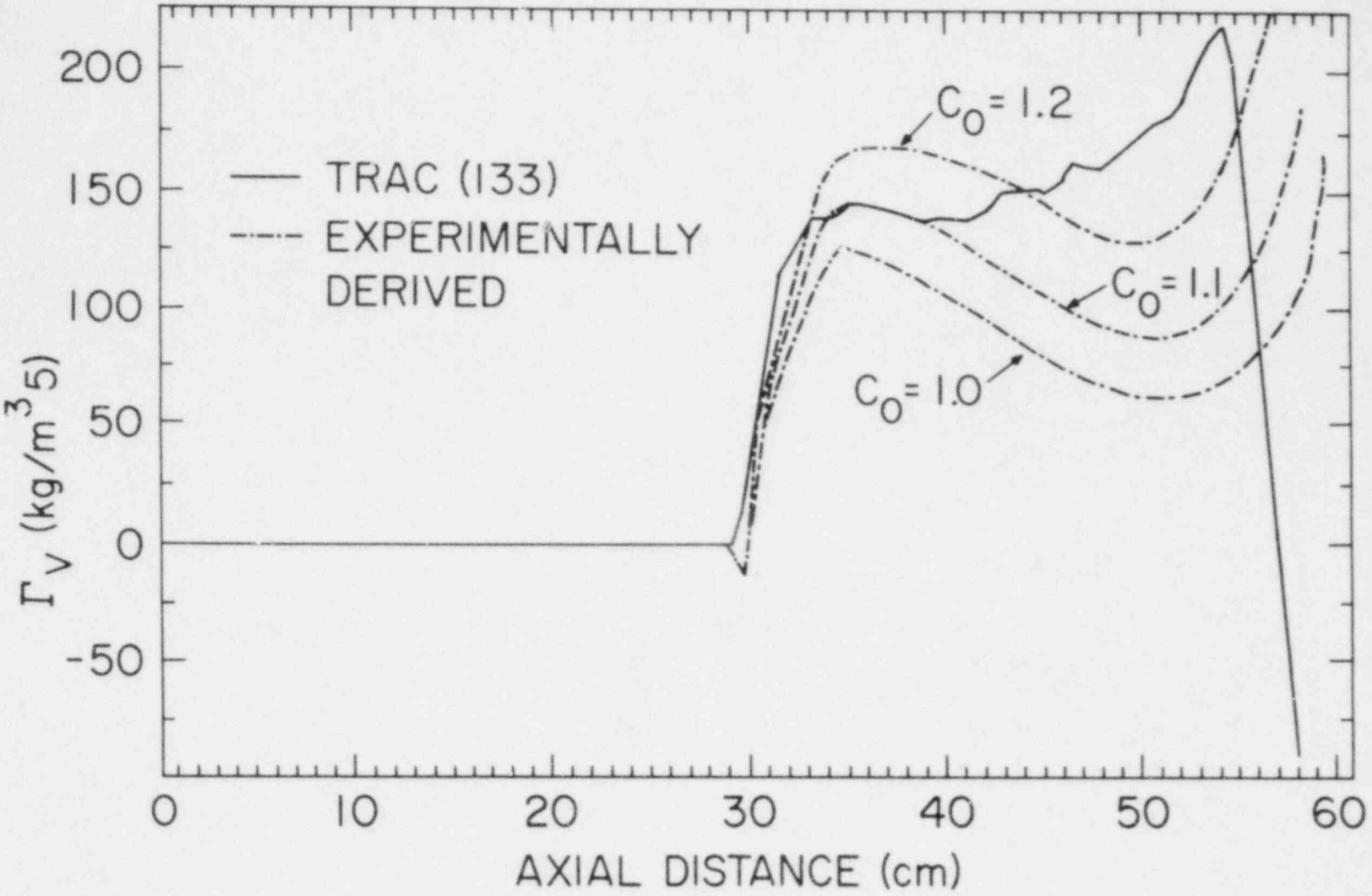

Figure 1.7. Comparison of vapor generation rates calculated from expereimental data with TRAC-P1A predictions. (BNL Neg. No. 5-278-80)

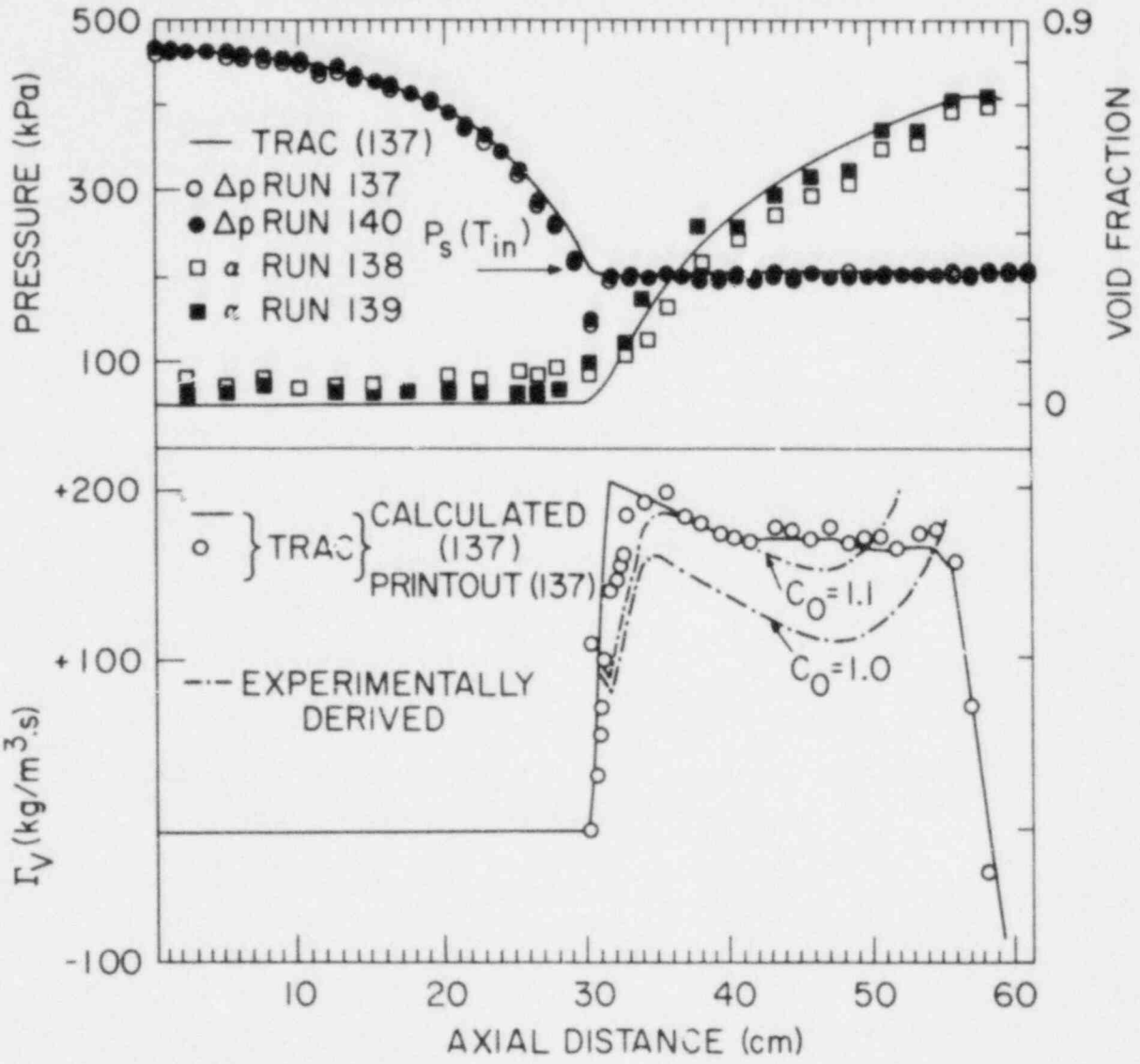

Figure 1.8. Comparison of experimentally measured pressure distributions and area averaged void profiles, as well as vapor generation rates calculated from the experimental data with TRAC-P1A predictions. (BNL Neg. No. 5-275-80)

TABLE 1.1

COMPARISON OF 121 C INLET TEMPERATURE RUNS
WITH TRAC PREDICTIONS

Run No	P_{in} (kPa)	T_{in} (C)	Flow Rate L/M	Exp. Mass Flow Rate kg/s	TRAC Mass Flow Rat kg/s	% Deviation
141	239.7 ± 4.9	121.3 ± 0.1	6.35 ± 0.01	5.98	4.84	-18.
144	242.5 ± 4.8	121.3 ± 0.1	6.33 ± 0.02	5.96		
145	306.2 ± 0.7	121.2 ± 0.1	7.92 ± 0.01	7.46	7.30	- 2.1
148	304.1 ± 0.6	121.2 ± 0.1	7.92 ± 0.01	7.46		
133	350.3 ± 0.7	121.3 ± 0.1	9.48 ± 0.01	8.93	8.37	- 6.4
136	347.9 ± 0.6	121.2 ± 0.1	9.50 ± 0.01	8.95		
140	465.2 ± 2.2	121.5 ± 0.1	12.67 ± 0.02	11.93	11.71	- 1.6
137	462.8 ± 1.5	121.8 ± 0.1	12.61 ± 0.02	11.87		

2.0 RAMONA-III, IRT and RETRAN Code Modification and Evaluation

The bulk of the effort with RAMONA-III this quarter dealt with code assessment. Comparisons were made with data from the Peach Bottom-2 (PB) Turbine Trip Tests and from heated channel experiments. Calculations of the PB tests were also compared with results from other codes for variables not measured. This analysis demonstrated that there were deficiencies in the neutronics and hydraulics modelling which could be rectified.

The void feedback of the cross section data was found to be too weak. Recommendations were made to change the formalism within the code to allow for the void dependence to be a function of exposure in order to obtain the proper void feedback. In the interim, the cross section parameterization and corresponding data from another code were used to facilitate the assessment using the PB data.

In order to obtain better values of slip and hence void fraction, the Bankoff-Jones slip correlation was implemented in the code. Comparisons with void fraction measurements along heated channels helped validate this change in model as well as parts of the existing hydraulics model.

The volumetric flow rate equation was changed by adding compressibility terms that had originally been neglected. With this change and the new slip model, RAMONA-III calculations of initial power distribution and average power during the transient were in good agreement with the data from the PB tests.

Two methods of tuning to obtain steady state conditions with the BNL jet pump-recirculation loop model have been evaluated and a recommendation was made for which to use in the future. The steamline model which had been developed originally as a stand-alone code was integrated into RAMONA-III. This model and other models that had been operating in different versions of the code were integrated into a single version.

2.1 RAMONA-III Jet Pump-Recirculation Loop Model

Two methods of tuning to obtain steady state conditions with the BNL jet pump-recirculation loop model present in the code have been evaluated by applying them to Peach Bottom Turbine Trip Tests 1 and 2.

In the first method, the main loop loss coefficients are held fixed and the jet pump head is adjusted to obtain the desired mass flow. The resultant jet pump head and the given pump M ratio (1.96) are then used to determine the pump suction and drive line loss coefficients (Diamond, 1980). For Test 1 the set of core loss coefficients were fixed at the values previously obtained for Test 3. The initial guess of the jet pump head was taken at the known value for Test 1, $1.724 \times 10^5 n/m^2$. This yielded a total steady state mass flow of 1.328×10^4 kg/s, while the desired value is 1.276×10^4 kg/s. Four steady state runs with different pump heads were required to obtain the correct mass flow at a pump head of 1.590×10^5 n/m^2, 8% lower than the actual value.

For Test 2 the core loss coefficients were again fixed at the Test 3 values and the initial pump head was the actual value $1.331 \times 10^5 n/m^2$. This yielded a steady state mass flow of 1.128×10^4 kg/s compared to a desired value of 1.044×10^4 kg/s. Four runs were again required to reach this mass flow with a pump head of $1.128 \times 10^5 n/m^2$, 15% less than the true value.

The second method consists of fixing the jet pump head and adjusting the core entrance loss coefficients to obtain the desired steady state mass flow. For Test 1, the jet pump head was fixed at the known steady state value, 1.724×10^5 n/m^2. The core entrance loss coefficients were initially taken as the Test 3 value set. This resulted in an initial steady state mass flow of 1.321×10^4 kg/s. Five runs with different core loss coefficients were required to obtain the desired mass flow of 1.275×10^4 kg/s. The resulting core loss coefficients were $\sim$ 27% greater than Test 3 values.

Test 2 was started with the same Test 3 loss coefficients and the known pump head of 1.331×10^5 n/m^2. This resulted in a mass flow of 1.115×10^4 kg/s, which was adjusted to the correct value of 1.044×10^4 kg/s by using different loss coefficients. The final core loss coefficients were 64% greater than Test 3 values.

For transient calculations, the core entrance and jet pump loss coefficients are held fixed at their steady state values. The relative power responses of both Turbine Trips 1 and 2 showed no appreciable difference between the two methods of obtaining steady state.

The method of adjusting the pump head is the simplest since only one number must change. However, differences of the order of 15% in pump head can be expected. On the other hand, the adjustment of the core inlet loss coefficients even though more complex, allows the correct value of pump head to be used while the loss coefficients themselves are not well known quantities.

2.2 RAMONA-III Steamline Model

The steamline model was integrated into the code. Many of the difficulties involved in doing this related to the blending of the integration scheme for the new model into that which existed in the code. A very complex and sophisticated time stepping is used in RAMONA-III which allows for different time steps for neutronics and thermal-hydraulics and allows backstepping in order to achieve certain criteria. Now that this has been accomplished, RAMONA-III is able to calculate the steamline pressure P_{SD} rather than have it imposed as a boundary condition. Results for P_{SD} are shown in Fig. 1 for Turbine Trip Test 3 at the Peach Bottom-2 Plant. The agreement is excellent out to the time of the peak power 0.7s, when the steamline dynamics dominate. This comparison, however, was done with a RAMONA-III void model and input deck which underpredicts the power rise during the transient (cf. Section 2.4). This underprediction will affect the agreement for $t > 0.7$s.

2.3 RAMONA-III Fuel Rod Modelling

A calculation was done with the heat transfer to the coolant held at the steady state value in order to study the sensitivity of the power peaking to the fuel rod heat conduction model. This calculation, which was expected to be an upper limit, resulted in a lower power peak relative to the case in which the new ScP fuel rod model was used. This is consistent with the observation that with the fuel rod model the heat transfer into the coolant actually decreased during the initial phase of the transient. A decrease in heat transfer helps reduce voids and (through feedback), therefore, increase power. The reason for the decrease related to the fact that in the boiling region of the core the heat transfer is proportional to the difference between clad surface temperature T_{ca} and saturation temperature T_{sat} to the fourth power. Initially as pressure increases T_{sat} increases faster than T_{ca} and the heat conduction is reduced.

2.4 RAMONA-III Code Assessment

2.4.1 General Results

The code assessment work continued aided by comparisons between RAMONA-III calculations and measurements of the Peach Bottom-2 Turbine Trip Tests, calculations of other codes, and heated channel experimental data. Previous analysis of the Peach Bottom (PB) tests (Diamond, 1980) underpredicted the rise in power observed during the transients. The cause for this had been identified as being a combination of deficiencies in the hydraulics modelling and the neutronics input data. The objectives of work during the present reporting period were to identify the problems more specifically and to take corrective action.

In order to demonstrate the importance of void feedback for a turbine trip transient a sensitivity calculation was done with the help of a point kinetics code. Reactivity as a function of time was input into the code and the resulting power trace was observed. The reactivity function was taken from a BNL-TWIGL calculation of Turbine Trip Test No. 3 (TT3) (Cheng, 1978). It had components due to void changes, moderator and fuel temperature changes and control rod movement. An arbitrary decrease in the void reactivity component by 20% reduced the peak power by 50%; thereby demonstrating the importance of void feedback.

2.4.2 Neutronics Considerations

The void reactivity feedback can be thought of as the product of a void reactivity coefficient ($\frac{\partial \kappa/\kappa}{\partial \bar{\alpha}}$) and a change in core average void fraction $\delta\bar{\alpha}$. Both of these factors are in turn functions of the void fraction $\bar{\alpha}$. The neutronics data that had been used in the original PB calculations had been generated by Scandpower, Inc. (ScP) under subcontract to BNL. The void dependence of the cross sections had been calculated at beginning-of-life for each of the fuel types in the core. The tests were actually performed at

end-of-cycle 2. Calculations at BNL and elsewhere have shown that the void feedback becomes stronger with exposure.

To demonstrate that the ScP cross sections had too weak a void dependence, they were used to calculate a void coefficient. The results were then compared with the void coefficient calculated using the cross sections from BNL-TWIGL since the latter code had successfully calculated the PB tests (Chen, 1978). The void coefficient was obtained by calculating a multiplication constant k from the two group data which is a function of void function. For the data that was being used in RAMONA-III, this was done for each of the three fuel types with and without control blades accounted for and for a range of exposures. For the BNL-TWIGL data, it was done for two (of the eleven) fuel compositions representing different exposures. The void coefficient $\frac{\partial \kappa/\kappa}{\partial \bar{\alpha}}$ as a function of void was typically twice as strong with the BNL-TWIGL data and had a stronger dependence on void fraction.

As a result of these studies, BNL has requested a change in the cross section parameterization within the code so that it can accept axial variation of the void dependence which is a function of both exposure and exposure weighted void history. The neutronic data to go with this new formalism has also been requested from ScP. Until that data becomes available, it was decided to pursue the code assessment work using the data that had been used in the two-dimensional BNL-TWIGL (B-T) study. The ability to apply that data in RAMONA-III had been developed previously (Diamond, 1979) but had never been utilized.

2.4.3 Hydraulics Modelling

In order to use the new (B-T) data, the hydraulic channel representation had to be changed in order for it to be consistent with the fact that the B-T data were derived for four-bundle rather the single bundle regions. New steady states were then obtained for each of the test conditions. This is done by adjusting the loss coefficients in the core in order to get the correct total mass flow. The bypass channel loss coefficient is adjusted to assure that the mass flow in that channel is correct relative to the total flow. (Sensitivity calculations demonstrated that the transient results were insensitive to these loss coefficients).

With the new (B-T) cross sections, RAMONA-III did give an increase in the peak power. However, the steady state average axial power distribution was shifted toward the bottom of the core. This was traced to the variance between axial void distributions in RAMONA-III and BNL-TWIGL. By artificially imposing the BNL-TWIGL void distribution (only), when computing the nodal cross sections, reasonable agreement was obtained for the power shape. The RAMONA-III calculated void distribution had been suspect even before these calculations because of its effect on void feedback as explained above. In addition, it had been noted that the initial core average void fraction calculated by RAMONA-III for TT3 had been ~ 0.36 whereas BNL-TWIGL, RETRAN, and ODYN had calculated $\sim 0.29 - 0.30$. Because of all this evidence, the hydraulic model was scrutinized.

Corresponding to the high values of void fraction were low values for slip. The Bankoff-Malnes (BM) correlation was the slip option being used in the core and riser. (There is also a correlation due to Solberg available). That slip model is described as follows:

$$v_g = S^{BM} v_f + v^o$$

$$S^{BM} = \kappa\ (1-\alpha)/(\kappa-\alpha)$$

where the notation is obvious and $\kappa = 0.904$ and $v^o = 0.147$ m/s were recommended for use by the code's developers. Another slip model of interest was the Bankoff-Jones (BJ) correlation which is used in BNL-TWIGL. That model is described by:

$$v_g = S^{BJ} v_f$$

$$S^{BJ} = (1-\alpha)/[\kappa(\alpha,P)-\alpha]$$

In order to evaluate the effect of a slip model close to the BJ model, the slip parameters in the BM model were changed to $\kappa = 0.825$ and $v^o = 0.001$ m/s. This resulted in a reduction in $\bar{\alpha}$ at steady state of 0.04 as well as a reduction in maximum transient power of $\sim$ 20%. The reduction in $\bar{\alpha}$ was sufficient to recommend the use of of the BJ correlation or the new parameters in the BM correlation.

The BJ model was inserted into RAMONA-III and showed a similar effect on $\bar{\alpha}$. In addition, the steady state average axial power distribution with the BJ correlation in place (and using the B-T cross section data) was much closer to the measured curve. (The agreement between the calculated and measured power shapes for all three tests was later improved by a single adjustment of the albedo parameters at the bottom of the core).

At this stage limited calculations of heated channel experiments were done in order to assure us that the thermal-hydraulic model with the new (BJ) slip model was doing an adequate job. A single core channel in the code was isolated from the remainder of the system. Immediately before the thermal-hydraulic calculation in this channel all the properties relative to the heated channel are inserted. This includes flow cross section area, flow rate, heated flux, heated length, heated perimeter, Dittus-Boelter and Jens-Lottes heat transfer coefficients, inlet temperature, pressure, specific heat, liquid density, vapor density, latent heat, and saturation temperature.

Calculations were done for three six-rod bundles (Eklund, 1965) and one 36-rod bundle (Nylund, 1968). In one set of calculations BM slip was used with $\kappa = 0.825$ and $v^o = 0.001$ m/s and in another set the BJ slip was employed. In all cases results for the void fraction along the heated channel were in reasonable agreement with the data. Figures 2 and 3 show the comparison for two of the tests. The solid line and the inverted triangles represent two independent calculations. The discrete points were obtained as just described. The solid line was obtained by following the description of

the void model given in the RAMONA-III documentation and then doing a "hand" calculation.

Another part of the hydraulics model is an option in the code which allows the hydraulic properties to be computed at the local pressure around the loop. This pressure is calculated by an inertia-free momentum equation. It should be noted that this option only affects properties and does not compute local values of the time rate of change of pressure, $\dot{P}$. Only one value of $\dot{P}$, the dome value, is used throughout the loop.

In order to use this option, corrections recommended by ScP were incorporated into the code. These modifications apparently smooth the pressure in the core and riser. With these updates in place, use of the local pressure option gave a steady state power distribution not significantly changed, an initial void fraction change of less than 0.01, an increase in inlet subcooling of 1°C and a decrease in power peak during the transient of $\sim$ 20%. Without the correction the option had more severe consequences. Because ScP had in the past some misgivings about this option (as evidenced by the recent update with corrections) and because the balance equations solved in RAMONA-III are not consistent with the use of local pressure dependent properties we are not recommending use of this option.

The expression for the divergence of mixture volume flux in the present version of RAMONA did not have any terms proportional to the time rate of change of pressure, $\dot{P}$. The $\dot{P}$ terms affect the volume flux divergence in two ways; the compressibility of the phases and the vapor generation, ψ. At this time, only the compressibility effects have been investigated. The vapor generation effects are approximately accounted for by the code's non-equilibrium void model and is left to investigation at a later time.

The equation for specific volume flow, W_k, out of section k including the compressibility effects but neglecting the rate of change of the specific phasic volumes with temperature is

$$W_k = \frac{w_{f,k-1}}{\rho_{f,k}} + \frac{w_{g,k-1}}{\rho_{g,k}} + \psi_k \left(\frac{1}{\rho_{g,k}} - \frac{1}{\rho_{f,k}}\right) + \frac{dP}{dt}\left[m_{f,k}\frac{\partial}{\partial P}\left(\frac{1}{\rho_{f,k}}\right) + m_{g,k}\frac{\partial}{\partial P}\left(\frac{1}{\rho_{g,k}}\right)\right]$$

where w is the mass flow rate and m_f and m_g are the mass of liquid and vapor.

The original version of RAMONA-III as received from Scanpower included the vapor compressibility term but not the liquid term. In a subsequent update, ScP removed this term because of a claim that use of the system (dome) rate of change of pressure as an approximation to the local rate of change of pressure in the equation could lead to erroneous results.

Investigation of the pressure time history of TT3 in both the dome and the core entrance showed no appreciable difference (except for delay) between the two locations. Therefore, since these terms are physically realistic, they were introduced into the code and their effects on TT3, with slip coefficients of $\kappa = 0.825$ and $v^\circ = 0.001$ m/s, were assessed. The vapor term alone was added first. This had the effect of reducing the relative peak power by only 1%. However, when the liquid compressibility term was added, the peak relative power increased 53%. This increase was traced to an observed increase of 0.002 in the change in average void between steady state and the time of peak relative power. This large effect of liquid compared to vapor compressibility at first seemed unrealistic. However, when one considers that the flow in the downcomer and lower plenum has zero void, rendering, $m_g = 0$ and m_f large, the volume flux at the core entrance is increased by about 5% due to liquid compressibility, leading to the observed void decrease in the core. It is therefore concluded that both of these compressiblity terms should be retained.

Another set of calculations were carried out to evaluate the sensitivity of the code to the trace of system pressure with time. All of the above calculations were carried out with the tabulated experimental dome pressure as the transient disturbance. To test the sensitivity to this pressure representation, several fits to this data were tested. The best fit, a polynomial which passes through the center of the data, yielded a peak relative power increase of $\sim$ 13% with the presence of the compressibility terms mentioned above. This again shows that the peak power is a very sensitive quantity and hence difficult to use for code evaluation.

2.4.4 Peach Bottom Results

RAMONA-III calculations have now been completed for all three turbine trip tests. They use an input function to describe the system pressure (core exit) as a function of time. Cross sections are from the BNL-TWIGL study and albedoes have been modified. Bankoff-Jones slip is used and the compressibility derivative terms are present in the equation for the volumetric flow rate. For all three tests, the steady state average axial power distribution and the core average power trace are in reasonable agreement with measurements.

Result for the power peak and time of peak are shown in Table I for all three tests. In order to obtain the same zero time point for calculation and experiment, the steam dome pressure imposed in the calculations (corrected for steam dome to core time delay) is lined up with the experimental trace. Based on our knowledge of many calculations of the power history, the agreement shown is quite good.

Table I

Maximum Relative Core Power

	Measured		Calculated	
	Power	Time, s	Power	Time, s
Test 1	5.18	.79	4.66	.78
Test 2	4.69	.73	5.27	.71
Test 3	4.93	.70	5.18	.68

2.5 Programming

An unpredictable fatal error which frequently prevented successful relaxation to steady state was identified. A fix was instituted which relates to protecting certain convergence tests from dividing by very small numbers. Other updates were added to the code in response to other problems identified at BNL and at ScP.

Several new models and calculational features which were developed independently have been integrated into one version of RAMONA-III. This includes: 1) the improved fuel rod model (ScP version); 2) the steamline model (as an option); 3) the critical power ratio calculation; 4) the plant protection system (19 functions); and 5) the plot file capability. In order to accommodate the additional coding, it was necessary to modify the code so that it could run using the BNL segmented loader.

2.6 IRT Code Modification and Evaluation

2.6.1 Once-Through Steam Generator Modelling - Mark II Version

The Mark II version of the IRT once-through steam generator has successfully run a transient (on a stand alone basis) and the results are in reasonably good agreement with the results from a similar transient calculated with the Mark I version. The equations for the downcomer and the aspirator flow between the downcomer and the tube region are included in the modelling. Initially, an instability was observed when the downcomer model was added. Detailed comparison with the Mark I modelling indicated that the momentum equation associated with the aspirator flow calculations caused this instability. (Since this momentum equation did not include an inertia term, instantaneous

aspirator flow reversals could be predicted). This equation was removed from the model and the aspirator flow was calculated in the same manner as in the Mark I version; this led to much more stable results. This model is currently being implemented in the IRT code.

Work was initiated on the implementation of a momentum equation in the IRT code. The model being added will calculate the main coolant flow rate based on friction, elevation, and main coolant pump pressure differences. This calculation will provide the flow rate at the exit of the pump where it was previously specified as a code input parameter.

Reorganization of the IRT code input was initiated. The input to the code is being modified so as to group logically connected parameters. For example, all steam generator parameters will be specified in one contiguous group of input numbers. Most of the current input parameters have been categorized and a code has been written to sort the input dictionary on these categories.

2.6.2 Once-Through Steam Generator Analysis

Work continued on the analysis of the overcooling transient for a typical B&W plant. Current analyses include the evaluation of the effects of feedwater temperature variation during the transient.

2.7 RETRAN Code Implementation and Verification

RETRAN code input decks have been obtained for the Sequoyah plant. The decks are set up for low power natural circulation calculations and for calculations at rated conditions. Both models have been run successfully on the BNL computer. Modifications necessary to simulate the first natural circulation test to be performed at the Sequoyah plant are being implemented.

A listing of the RETRAN input for the Trojan plant has been obtained from the Portland General Electric Company.

REFERENCES

I:AMOND, D. J., et al., "Water Reactor Safety Research Division, Quarterly Progress Report," April 1 - June 30, 1979, BNL-NUREG-51081 (1979).

DIAMOND, D. J., et al., "Water Reactor Safety Research Division, Quarterly Progress Report," Oct. 1 - Dec. 31, 1979, In press (1980).

CHENG, H. S., DIAMOND, D. J., "Core Analysis of Peach Bottom-2 Turbine Trip Tests," BNL-NUREG-24903 (1978).

EKLUND, R., GELIUS, O., NYLUND, O., ASEA-PM-KAB 65-8, ASEA-Atom, Vasteras, Sweden (1965).

NYLUND, O., et al., "Hydrodynamic and Heat Transfer Measurements on a Full-Scale Simulated 36-rod Marviken Fuel Element with Uniform Heat Flux," FRIGG-2 AB Atomergi, Stockholm, Sweden (1968).

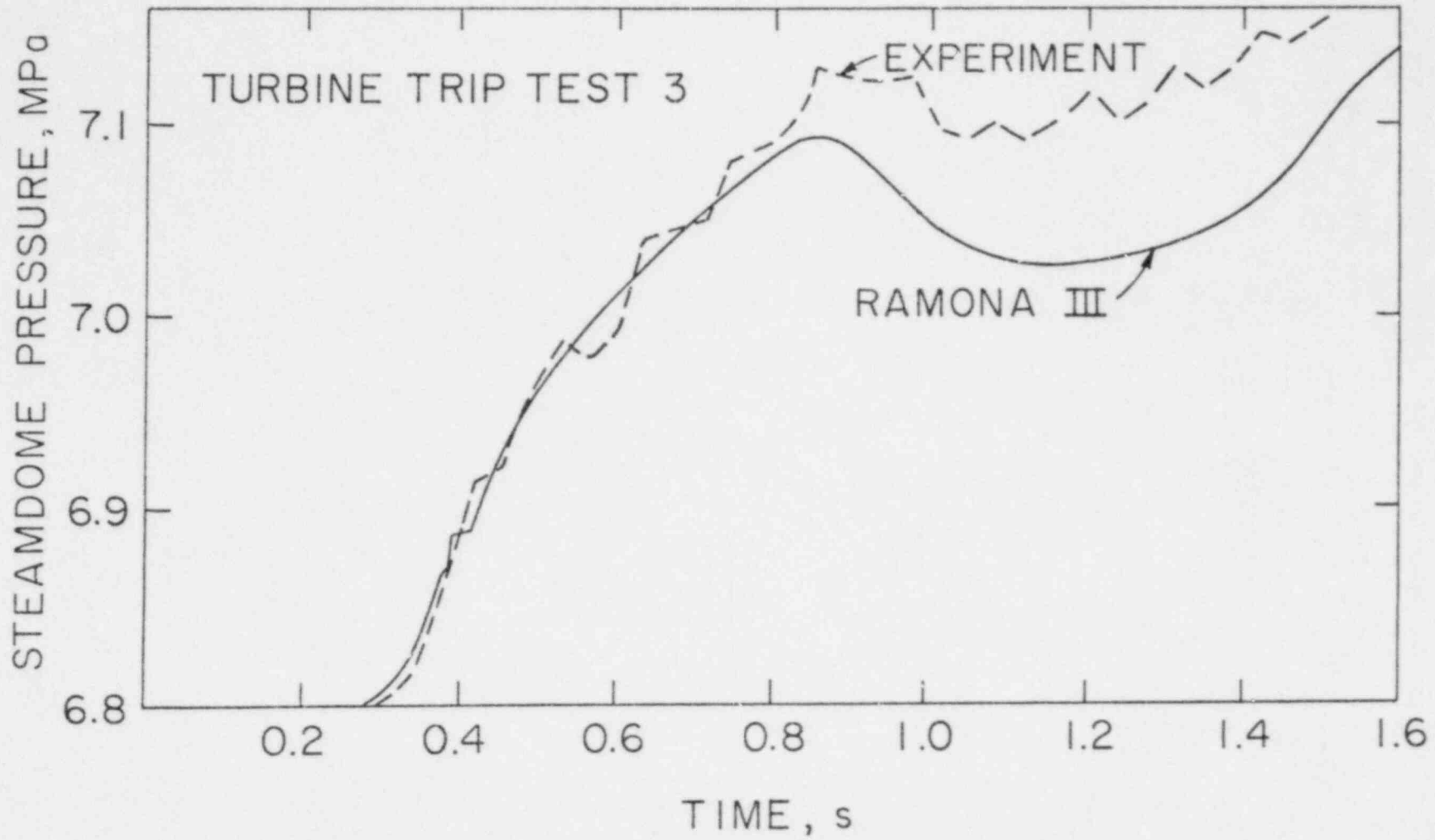

Figure 1

Steamdome Pressure for TT3

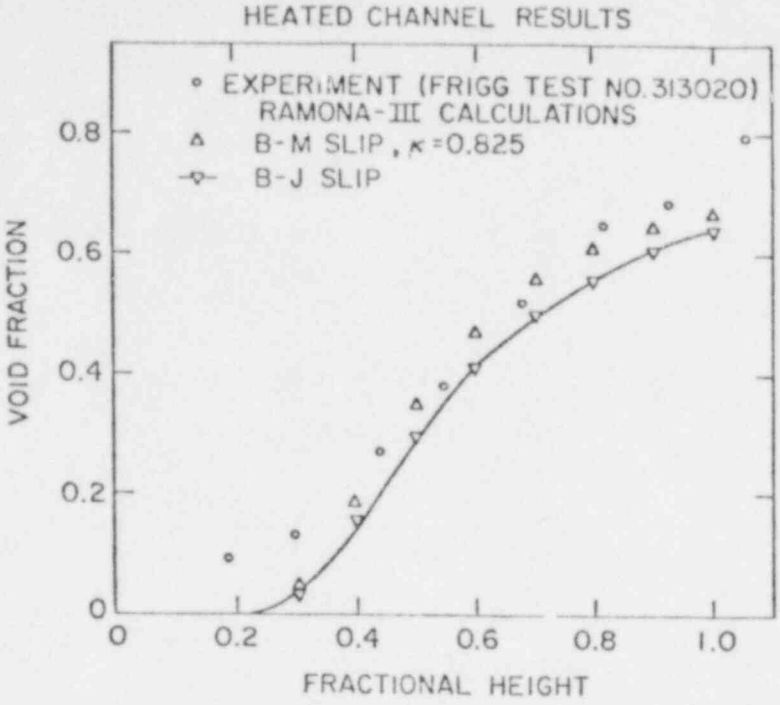

Figure 2

Comparison of Measured and
Calculated Heated Channel Data

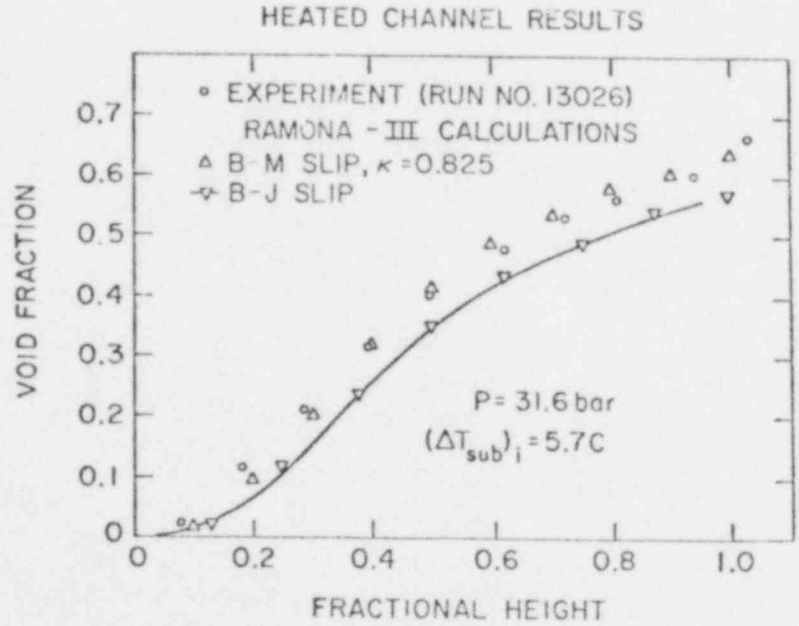

Figure 3

Comparison of Measured and
Calculated Heated Channel Data

4. TRAC Assessment and Model Improvement

4.1 Moby-Dick Nitrogen-Water Experiments (P. Saha)

The TRAC-P1A assessment work with the Moby-Dick nitrogen-water tests (Jeandey, 1979) continued during the reporting quarter. It was mentioned in the previous quarterly report (Saha, 1980) that an entrance loss, which was not modeled in the TRAC calculations, seemed to exist at the inlet of the test section. Instead of having to specify an added frictional loss at the inlet, it was decided to start the simulated test section 0.3m downstream of the actual entrance and use the experimental pressure at that location as the boundary condition for the revised TRAC calculations. Also, the nitrogen gas properties are used instead of the air properties for these latest calculations. All the NRC-specified tests and two additional tests (Run 3167 and 3052) have been run with the above input changes, and the results are described below.

Figure 4.1 shows the TRAC-P1A predictions with the experimental data for the zero quality run, i.e., Run 3095. Two different friction factor options were used. The homogeneous friction factor option used a smooth wall, Blasius-type single-phase friction factor correlation, whereas the annular friction factor option used a rough wall, Colebrook-type single-phase friction factor with roughness heights equal to 5×10^{-6}m. These two options, as available in TRAC, produced significantly different mass flow rates and axial pressure distributions as seen in Figure 4.1. The experimental value of the mass flow rate is in between the two TRAC predictions. This shows the importance of specifying the correct single-phase friction factor which, from experiments, has been found to lie between the smooth wall and the rough wall friction factor values.

The various two-phase runs have been simulated by specifying the experimental mass flow rate of nitrogen through the injection nozzle. The code, however, predicts the water mass flow rate for the given experimental pressure boundary conditions. Various two-phase friction factor options have been used which resulted in different TRAC predictions for the water flow rate for the same test. Thus the calculated flow quality was also different. These results have been presented in Figure 4.2 and Table 4.1. It is seen that the annular and the Chisholm friction factor options, which use the rough wall single-phase friction factor correlation, usually underpredict the water flow rate and, consequently, overpredict the flow quality. On the other hand the CISE correlation overpredicts the water flow rate by as much as 50%. The homogeneous and the Armand friction factor options use the smooth wall single-phase friction factor option and both of them overpredict the water flow rate. This shows the sensitivity of the two-phase friction factors on the prediction of water flow rate.

A comparison between the TRAC prediction of axial pressure distribution and the experimental data for Run 3177 is shown in Figure 4.3. This is the only NRC-specified run for which the experimental data for both pressure and void fraction are available. It is seen from Figure 4.3 that, on the whole, a good agreement between the data and the TRAC pressure predictions is obtained. A magnified view of the comparison near the throat of the test section is shown in Figure 4.4. Although some differences between the data and the predictions do exist, they cannot be considered as large. Even between the two predictions

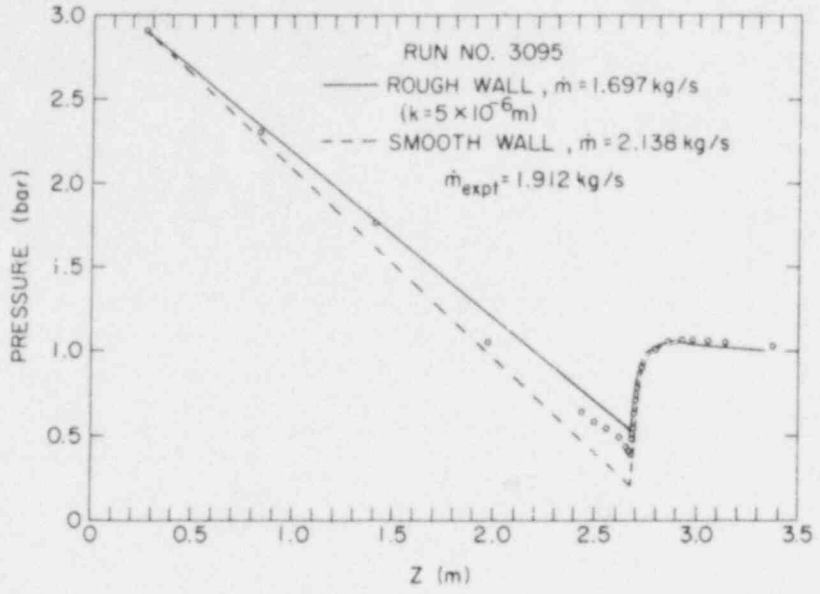

Fig. 4.1 Comparison of TRAC-PlA predictions with the Moby-Dick experiment with no nitrogen injection. (BNL Neg. No. 4-1341-80).

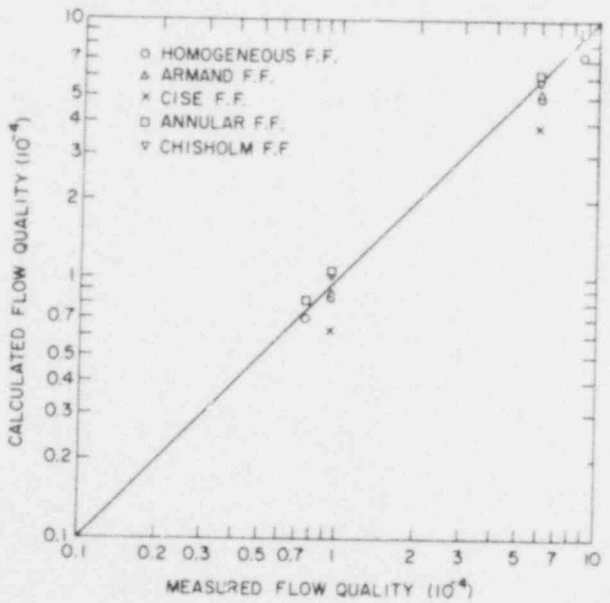

Fig. 4.2 Comparison of Calculated and Measured Flow Qualities for Various Two-Phase Friction Factor Options. (BNL Neg. No. 4-1340-80).

TABLE 4.1 SUMMARY OF MOBY-DICK NITROGEN-WATER TEST RESULTS

RUN NO.	MEASURED FLOW QUALITY (X)	WATER MASS FLOW RATE (kg/s)				
		EXPT.	TRAC CALC. (ANNULAR F.F.)	ERROR (%)	TRAC CALC. (HOMOGENEOUS F.F.)	ERROR (%)
3095	0	1.912	1.697	-11.2	2.138	+11.8
3176	0.94×10^{-4}	2.057	1.829	-11.1	2.259	+ 9.9
3177	0.93×10^{-4}	2.063	1.925	- 6.7	2.27	+10.0
3087	5.91×10^{-4}	1.915	1.822	- 4.9	2.251	+17.5
3089	5.90×10^{-4}	1.918	1.849	- 3.6	-	-
3091	5.95×10^{-4}	1.915	1.846	- 3.6	-	-
3141	51.3×10^{-4}	1.222	.....DID NOT CONVERGE TO A STEADY-STATE.....			
3167	0.75×10^{-4}	2.634	2.390	- 9.3	2.81	+ 6.7
3052	8.72×10^{-4}	1.929	1.865	- 3.3	2.289	+18.5

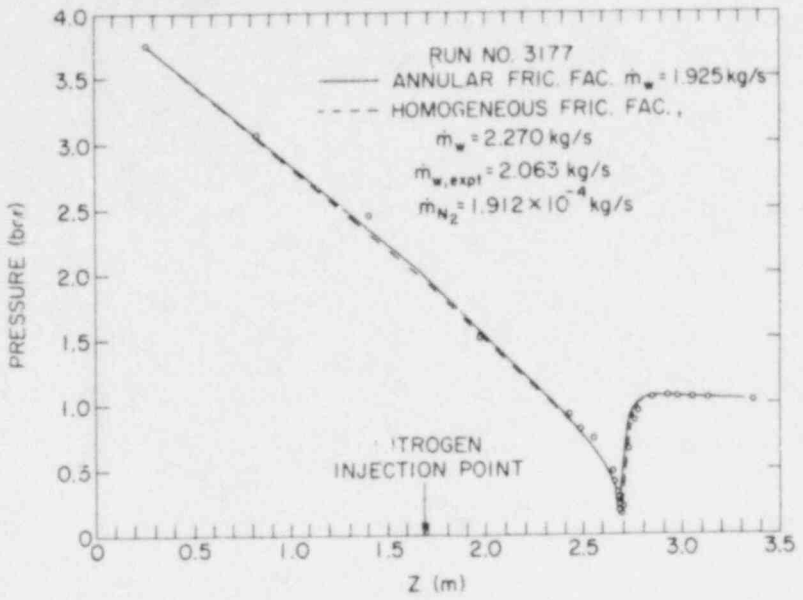

Fig. 4.3 Comparison of TRAC-P1A Pressure Predictions with the Moby-Dick Run No. 3177. BNL Neg. No. 4-1342-80).

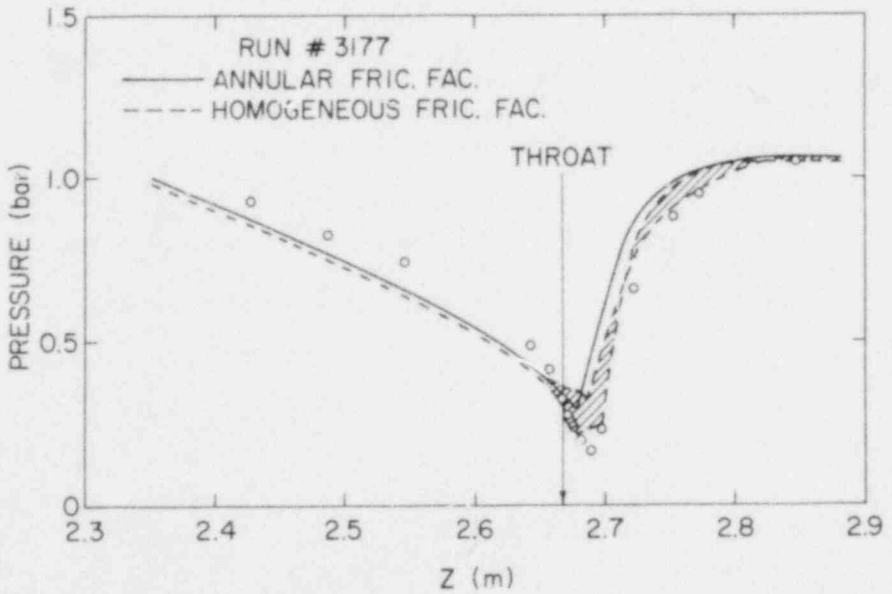

Fig. 4.4 Magnified view of the Pressure Predictions near the throat for Moby Dick Run No. 3177. (BNL Neg. No. 4-1345-80).

i.e., with the annular flow friction factor and the homogeneous friction factor the difference in axial pressures is quite small, although the difference in water flow rates is as much as 16.7% (see Table 4.1). This implies that the comparison with the pressure data alone is not sufficient for a critical evaluation of the TRAC code.

A comparison between the void fraction data and the predictions for Run 3177 has been made in Figure 4.5. Unfortunately, all the void fraction data with the exception of that at Z = 2.328 m, are the diametral-averaged void data and not the area-averaged data which are really needed for a meaningful comparison with the code predictions. The relationship between the diametral and area-averaged void fractions depends on the flow pattern which is not known for these experiments. For the two extreme flow regions, i.e., the annular flow and the inverted annular flow, the area-averaged void fractions $\langle\alpha\rangle$ can be determined by

$$\langle\alpha\rangle = (\alpha_c)^2 \qquad \text{(for annular flow)}$$

and

$$\langle\alpha\rangle = \alpha_c\,(2-\alpha_c) \qquad \text{(for inverted annular flow)}$$

where α_c is the diametral-averaged void fraction. Therefore, the value of the area-averaged void fraction can vary between α_c^2 and $\alpha_c(2-\alpha_c)$. For a diametral void fraction of 0.5, the area-averaged void fraction, therefore, can vary from 0.25 to 0.75, a rather large range.

Looking back to Figure 4.5, one can see that all the measured diametral void fractions are consistently higher than the predicted (area-averaged) void fractions. If an annular flow regime is assumed, the inferred area-averaged void fraction would come closer to the predictions. However, if a uniform radial distribution for the voids is assumed, i.e., $\langle\alpha\rangle = \alpha_c$, the code would significantly underpredict the area-averaged void data. Similar conclusions can be drawn from Figure 4.6 where the data of Run 3052 are compared with the TRAC predictions. Therefore, a proper verification of the TRAC slip models is not possible with the present Moby-Dick nitrogen-water data because of the lack of the area-averaged void fraction measurements. However, analysis with the "correct" single-phase friction factor will be done to complete the present assessment effort.

4.2 KFK-IRE Nozzle Flow Tests (P. Saha)

All three NRC-specified tests conducted in the KFK-IRE horizontal nozzle (Kedziur, 1978) have been simulated by TRAC-P1A. The test section consists of a short (0.6m) converging nozzle followed by a long (0.675m) straight pipe section. The inside diameter of the test section changes from 0.08m to 0.016m in the converging part, and then remains unchanged. In the previous BNL study (Srikantiah, 1979), it was shown that 85 cells were adequate to simulate this test section. The same nodalization scheme has been retained in the present analysis.

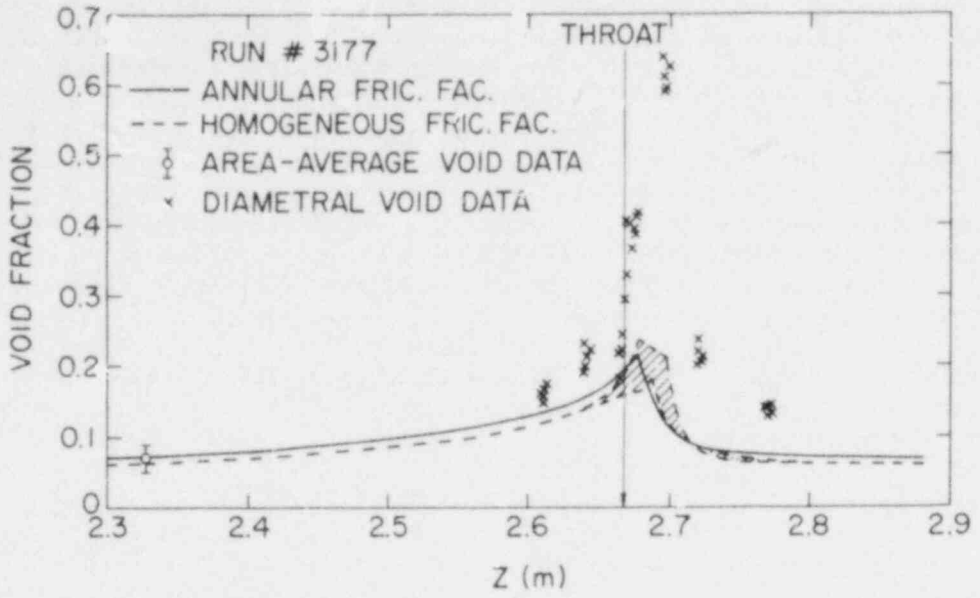

Fig. 4.5 Comparison of TRAC-P1A Predictions with the Void Fraction Data of Moby-Dick Run No. 3177. (BNL Neg. No. 4-1338-80).

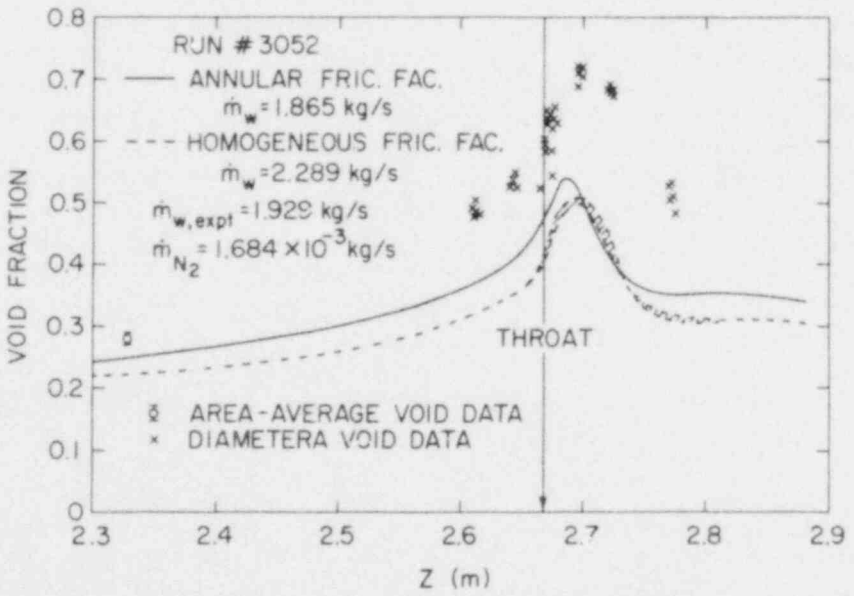

Fig. 4.6 Comparison of TRAC-P1A Predictions with the Void Fraction Data of Moby-Dick Run No. 3177. (BNL Neg. No. 4-1336-80).

The first test V02.08.78/13.59 was a "cold water" run. Only single-phase room-temperature water flowed through the nozzle. The test was simulated by specifying the pressure boundary conditions at both ends of a PIPE component. The mass flow rate and the axial pressure distribution are calculated by using two different friction factor options. The results are shown in Figure 4.7 and Table 4.2. It is seen that the TRAC prediction using the smooth wall single-phase friction factor, i.e., the homogeneous friction factor option is in better agreement with the experimental data than that using the rough wall or the annular friction factor option. This implies that the surface roughness of the KFK-IRE nozzle is most probably negligible and the calculation of the two-phase friction factor, when needed, should be based on a smooth-wall single-phase friction factor correlation.

The second test V02.08.78/15.20 was a room temperature air-water test. A two-phase air-water mixture with a flow quality of 1.21% was introduced through the inlet. In addition to the pressure boundary conditions, TRAC requires the inlet void fraction which was not measured. An inlet void fraction of 0.5054 was used as input. This value was computed from the measured flow quality of 0.0121 and the TRAC void distribution parameter, C_o, equal to 1.1. The results of the TRAC predictions, using the homogeneous and the annular friction factor options, are compared with the experimental data in Figure 4.8 and Table 4.2. None of the TRAC calculations show good agreement with the experimental data. Both the semi-implicit and the implicit numerical schemes were employed, and both yielded virtually the same results.

An analysis of the void fraction data showed that the experimental values of the void distribution parameter, C_o, and the slip ratio, S, seemed to decrease along the length of the test section. TRAC-P1A, however, uses a constant value of C_o, and because of the lower downstream pressure, the slip ratio in TRAC calculations increases along the length of the nozzle. These results are shown in Table 4.3. The correlation of Ishii (1977) for the void distribution parameter, i.e. $C_o = 1.2-0.2\sqrt{\rho_g/\rho_\ell}$, has also been examined in that Table. It is seen that according to the Ishii correlation, the value of C_o increases slightly along the length because of the decreasing pressure. The slip ratio also shows some increases. This is in contrast with the experimental values. Therefore, it is concluded that more air-water tests should be analyzed to establish the real trend of the distribution parameter and the slip ratio in this particular test section, and if needed, a new correlation for the relative velocity might have to be developed.

The last test V15.09.78/11.11 was a high pressure high temperature steam-water test. A two-phase steam-water mixture at 51.88 bar and 8.3% flow quality entered the test section. An inlet void fraction of 0.6617 was computed from the measured flow quality and the TRAC void distribution parameter, C_o, equal to 1.1, and was used in the TRAC input. Both the semi-implicit and the implicit numerical schemes were employed. However, the results obtained by the implicit method showed a sudden jump in void fraction at the entrance. This was similar to the earlier observations made at BNL (Srikantiah, 1979). The semi-implicit method did not produce such jumps. Therefore, only the results obtained by the semi-implicit method are compared with the experimental data in Figure 4.9 and Table 4.2. Again, the overall TRAC predictions were not very satisfactory, although the void fraction predictions seemed to be somewhat

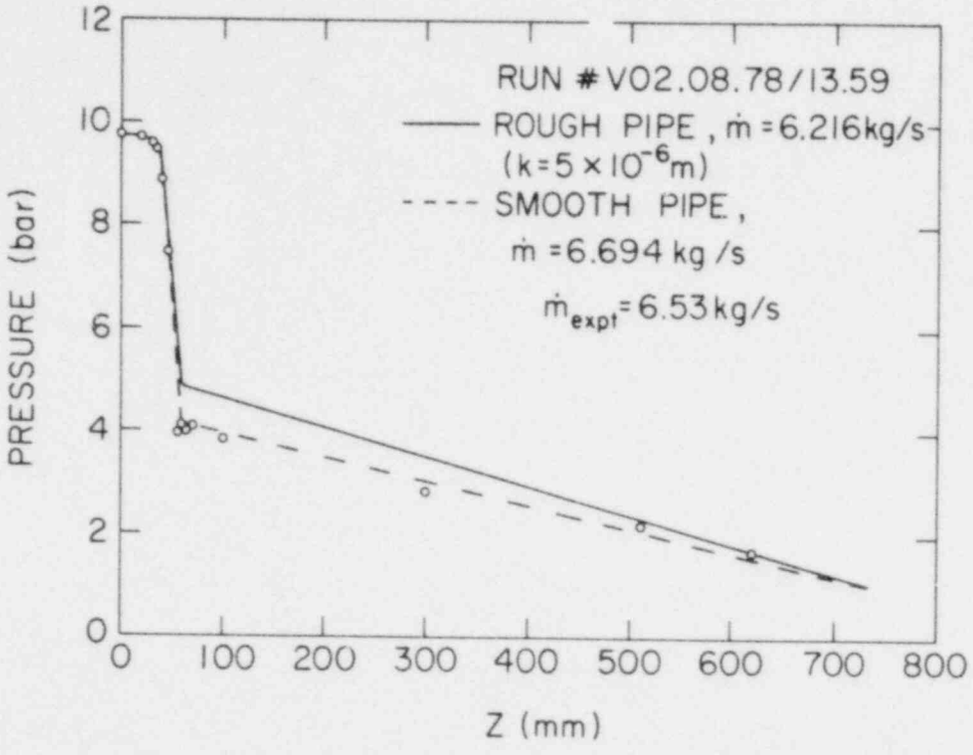

Figure 4.7 Comparison of TRAC-P1A Predictions with the KFK-IRE Cold Water Test. (BNL Neg. No. 4-1316-80).

Table 4.2 SUMMARY OF KFK-IRE TEST RESULTS

Run Number	Inlet Flow Qual.	Mass Flow Rate (kg/s) Expt.	TRAC Calc. (Annular F.F.)	Error (%)	TRAC Calc. (Homogeneous F.F.)	Error (%)
V02.08.78/ 13.59 (Cold Water)	0	6.53	6.216	-5.1	6.694	+ 2.5
V02.08.78/ 15.20 (Air-Water)	0.0121	2.32	2.128	-8.3	2.642	+13.9
V15.07.78/ 11.11 (Steam-Water)	0.083	3.065	2.816	-8.1	3.771	+23.0

Table 4.3 ANALYSIS OF VOID DATA FOR KFK-IRE AIR-WATER TEST V02.78.73/15.20

Item	Z = 60 mm		Z = 500 mm	
	C_o	S	C_o	S
1. Experimental Value	1.190	1.470	1.019	1.067
2. TRAC - P1A	1.10	1.247	1.10	1.349
3. ISHII	1.182	1.450	1.186	1.649

Note: $X = 0.0121$ ρ_v (Z = 60) = 8.3 kg/m^3

$\rho_\ell = 996$ kg/m^3 ρ_v (Z = 500) = 4.9 kg/m^3

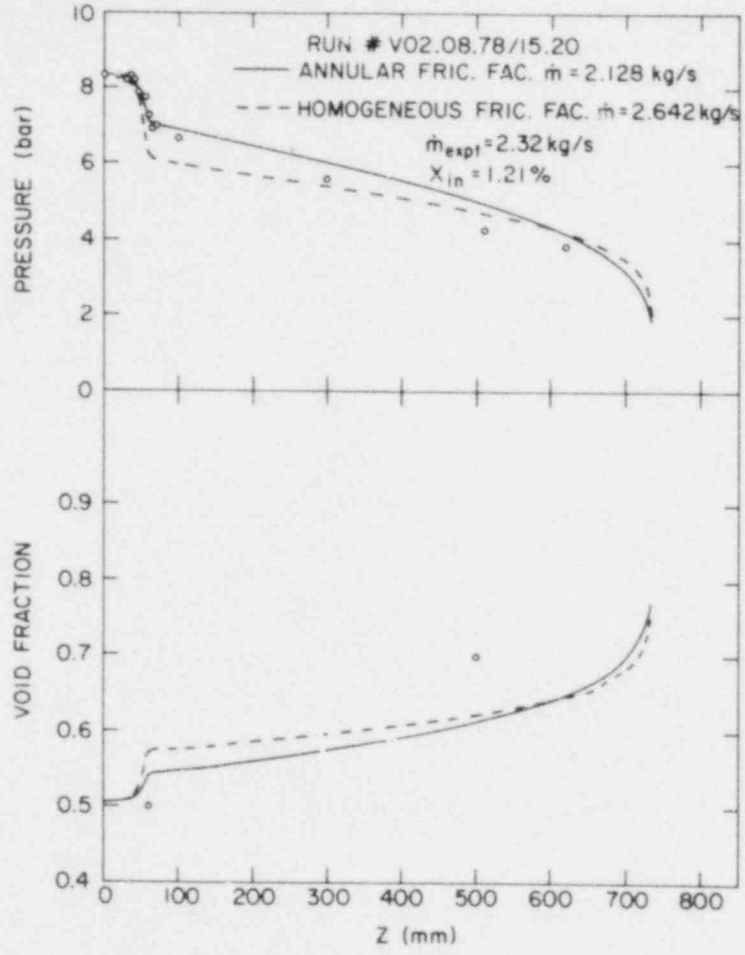

Fig. 4.8 Comparison of TRAC-P1A Predictions with the KFK-IRE Air-Water Test. (BNL Neg. No. 4-1321-80).

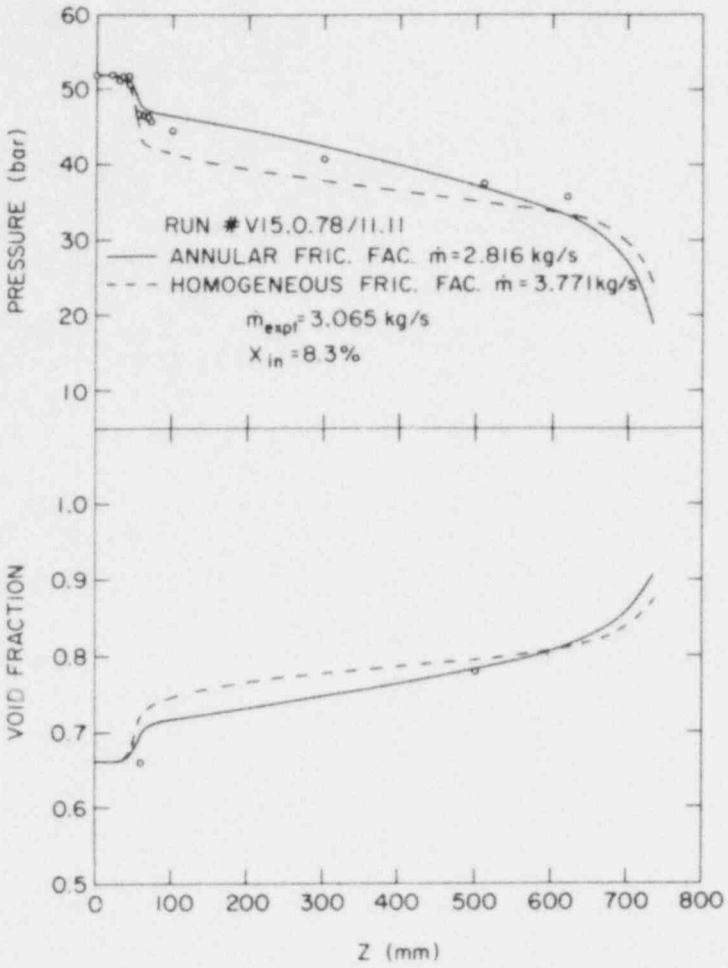

Fig. 4.9 Comparison of TRAC-P1A Predictions with the KFK-IRE Steam-Water Test. (BNL Neg. No. 4-1322-80).

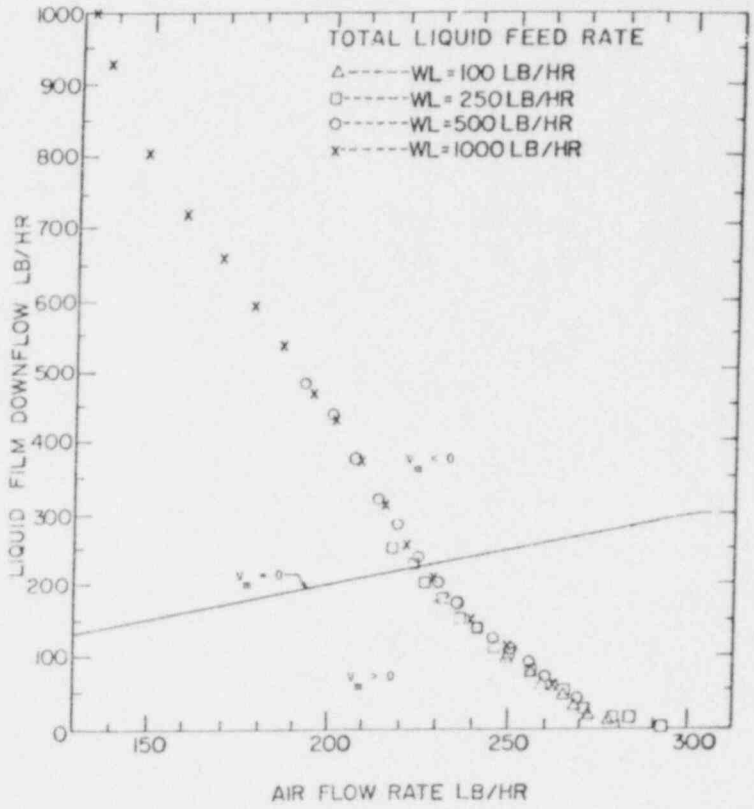

Fig. 4.10 Operating Region of the University of Houston Flooding Tests. (BNL Neg. No. 4-1318-80).

better than those for the air-water test. This may be due to compensating errors in the calculation of relative velocity and the nonequilibrium phase change rate.

4.3 Counter Current Flow Tests at University of Houston (U.S. Rohatgi)

These tests were conducted to study the flooding mechanism. The test section consists of a 4.12m long vertical tube of 0.051m I.D. It has a 0.102m section of porous sintered monel tube located at 2.013m from the top for introducing water uniformly. This test section is flared at the bottom and is connected to the chamber, in which air is introduced through a vertical nozzle. The liquid which is flowing down the test section is collected at the bottom of this chamber. The top of the test section is connected to a separator to separate water from the air. The details of these tests and the data are given elsewhere (Dukler et al 1977).

The TRAC-P1A assessment with these tests will be done by constructing curves showing liquid downflow as a function of air flow for various liquid inflow conditions. However, each point on these curves will come from a separate run of TRAC-P1A, which will be very expensive if the vessel module is used. Therefore, it has been decided to use the one-dimensional Pipe and Tee components to model these tests. This method of simulation will allow us to check the slip formulation in TRAC-P1A for countercurrent flow conditions. Furthermore, from the film thickness measurements, it was found that the void fraction in the test section was always greater than 80%. This means that only the annular regime drift description will be used and is given here as described in TRAC-P1A

$$V_r = \frac{V_m}{\left[\frac{\rho_g (76 - 75\alpha)}{\rho_\ell \sqrt{\alpha}}\right]^{1/2} + \frac{\alpha \rho_g}{\rho_m}}$$

We find from this expression that the relative velocity, V_r, and the mixture velocity, V_m, have the same sign so for flow conditions (mainly counter current) where V_m is negative this expression will give a wrong sign for V_r. Figure 4.10 shows the experimental data for liquid film downflow as a function of air flow for various liquid inflows. The straight line drawn in that figure represents the Equation $V_m = 0$. In the region above this line, V_m will be negative and TRAC-P1A will not yield correct results. Therefore, we will only attempt to predict the experimental data below this line. An input deck consisting of two TEEs, three FILLs, and one BREAK at the top, has been set up and is currently being debu

4.4 Super-CANON Experiments (P. Saha)

The Super-CANON tests (Riegel, 1979) were the high-pressure blowdown tests from a horizontal straight pipe. The pipe inside diameter was 0.1m and the length was 4.389m. One end of the pipe was closed, whereas the other end was ruptured to initiate the blowdown. The diameter of the open end was varied

from full-open (0.1m) to 0.03m. Initially, the test section was pressurized to 150 bar with subcooled water at 280°C - 320°C. As the transient progressed, the pressure and temperature at several positions, and the area-averaged void fraction at one station were recorded.

First, a nodalization study was performed. The test with full opening and maximum subcooling, i.e., $T_{\ell,in}$ = 280°C, was taken as the test case. Calculations with TRAC-P1A were conducted for four different nodalizations with total number of cells ranging from 52 to 160. In all nodalizations, finer cells were used near the break, and coarser cells were used upstream. Figures 4.11 and 4.12 show the calculated exit mass flow rates for different nodalizations. It can be seen that the effect of nodalization is rather small and it is primarily confined within the first 50 milliseconds or so. Therefore, as a compromise between the extreme accuracy and the long computation time, the nodalization with 104 cells has been adopted for all Super-CANON runs. This nodalization is comprised of 84 cells each of 0.05m in length, 18 cells each of 0.01m in length, and two 0.0045m long cells at the break.

Four Super-CANON tests have been simulated with TRAC-P1A. They consist of two different break diameters (0.1m and 0.03m) and two different initial water temperatures (280°C and 320°C). Figures 4.13 and 4.14 show typical results for the run with $T_{\ell,in}$ = 280°C and 0.1m break diameter. The pressure and the void fraction measurement stations were close to each other. It can be seen clearly from Figure 4.13 that the TRAC prediction is not in total agreement with the data. In particular, the TRAC overpredicts the pressure in the early part and underpredicts the same in the later part of the transient. This also implies that TRAC-P1A tends to empty the pipe sooner than the experiment.

Similar results were obtained for the other three runs. Figures 4.15 and 4.16 show the typical results for the test with $T_{\ell,in}$ = 320°C and 0.1m break diameter. Figures 4.17 and 4.18 show the pressure traces for the tests with 0.03m break diameter which prolonged the transient. However, in all of these figures, the same trend can be observed. Future studies will focus on the sensitivity of the various thermal-hydraulic models used in TRAC, and the areas where improved modeling might be needed.

4.5 Marviken Critical Flow Tests (U.S. Rohatgi)

Marviken Critical Flow Tests 20, 21 and 23 (Ericson, et al, 1979) were simulated in this quarter. These tests differ in initial temperature profiles, initial subcooling and length of the nozzle. The results of Tests 22 and 24 have been reported earlier (Rohatgi, 1980a) and will be used here for comparison. Tests 20, 21 and 22 have the same nozzle L/D of 1.5 but different subcooling of 7°C, 33°C and 52°C, respectively. These tests will show the effect of subcooling on the discharge flow rate and the conditions inside the test vessel. Tests 23 and 24 have smaller nozzle L/D of 0.33 and have subcooling of 5°C and 33°C, respectively. These two tests will show the effect of subcooling with smaller nozzle length. Furthermore, a comparison of Tests 21 and 24 will show the effect of nozzle length on flow conditions for the same subcooling. Note that all the nozzles had the same diameter of 0.5m.

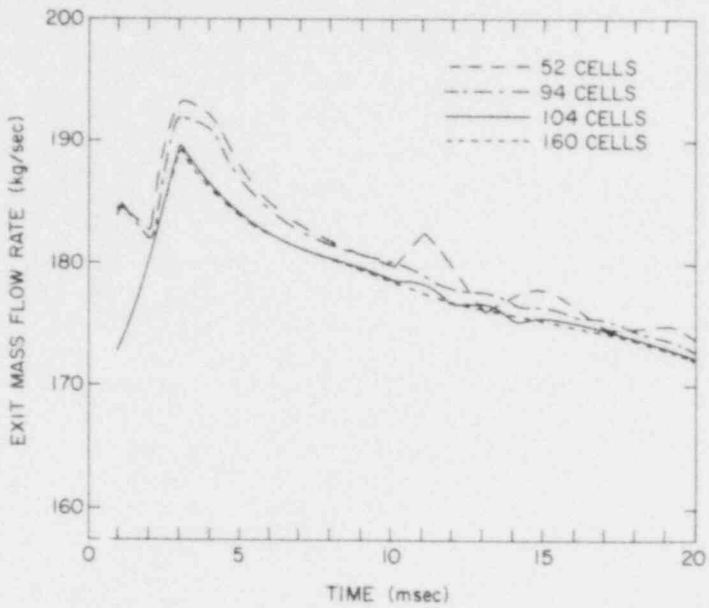

Fig. 4.11 Short Term TRAC-P1A Calculations of a Super-CANON Test for Various Nodalizations. (BNL Neg. No. 4-1337-80).

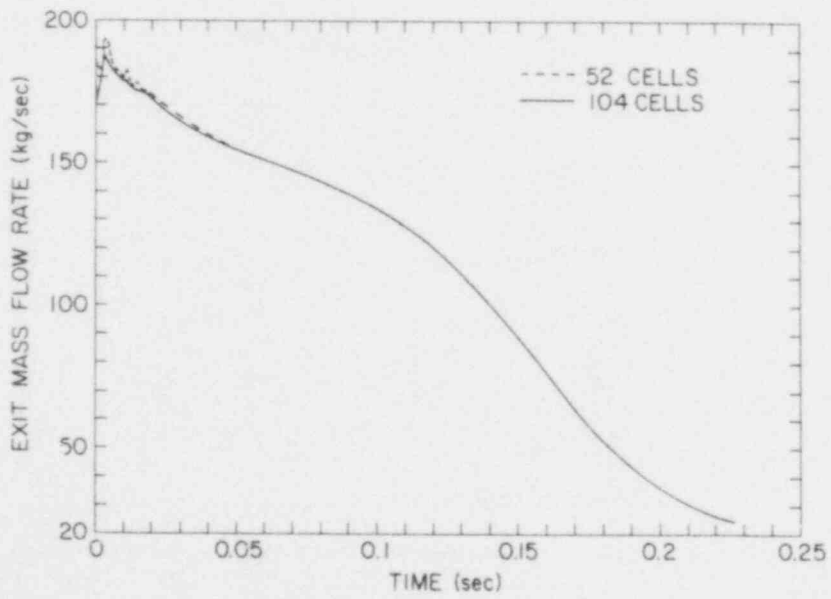

Fig. 4.12 Long Term TRAC-P1A Calculations of a Super-CANON Test for Various Nodalizations. (BNL Neg. No. 4-1339-80).

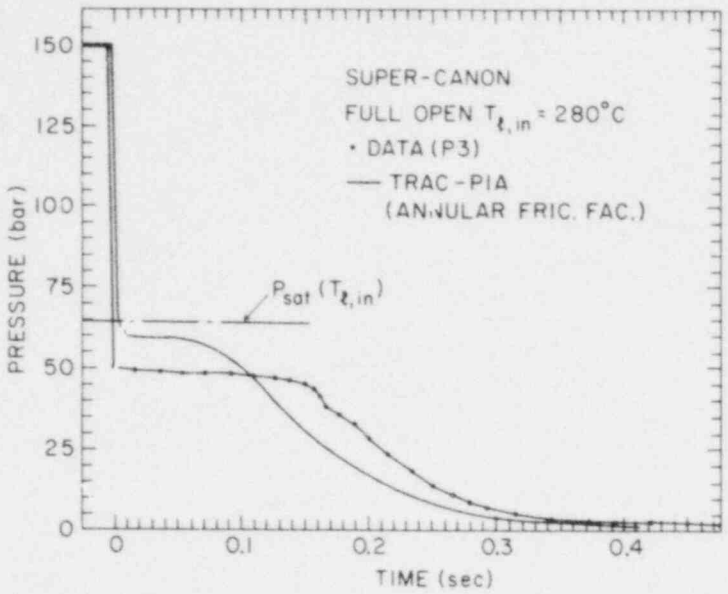

Fig. 4.13 Comparison of TRAC-P1A Prediction with the Pressure Trace of the Super-CANON Test with Full Open Exit and $T_{\ell,in}$ = 280° C. (BNL Neg. No. 4-1333-80).

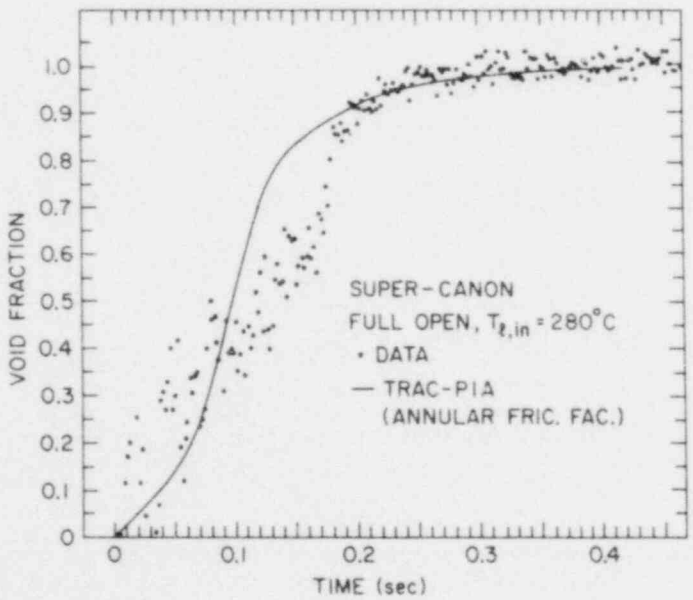

Fig. 4.14 Comparison of TRAC-P1A Prediction with the Void Fraction Data of of the Super-CANON test with Full Open Exit and $T_{\ell,in}$ = 280° C. (BNL Neg. No. 4-1335-80).

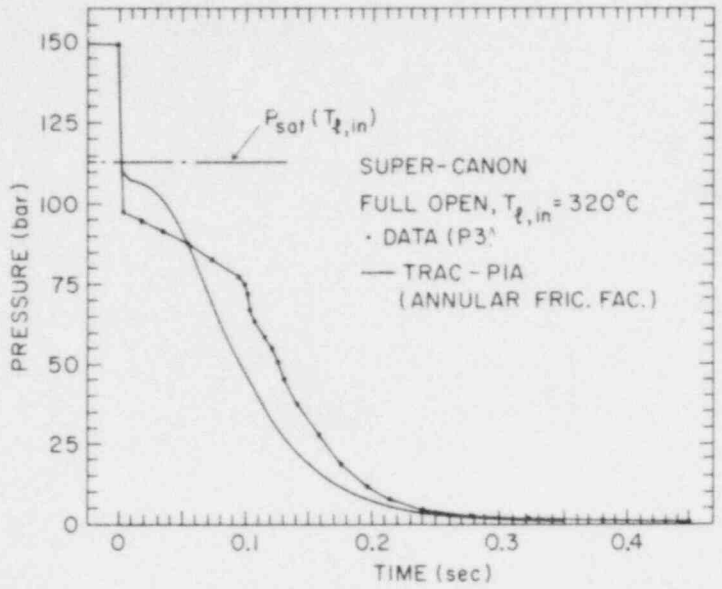

Fig. 4.15 Comparison of TRAC-PlA Prediction with the Pressure Trace of the Super-CANON Test with Full Open Exit and $T_{\ell,in}$ = 320° C. (BNL Neg. No. 4-1332-80).

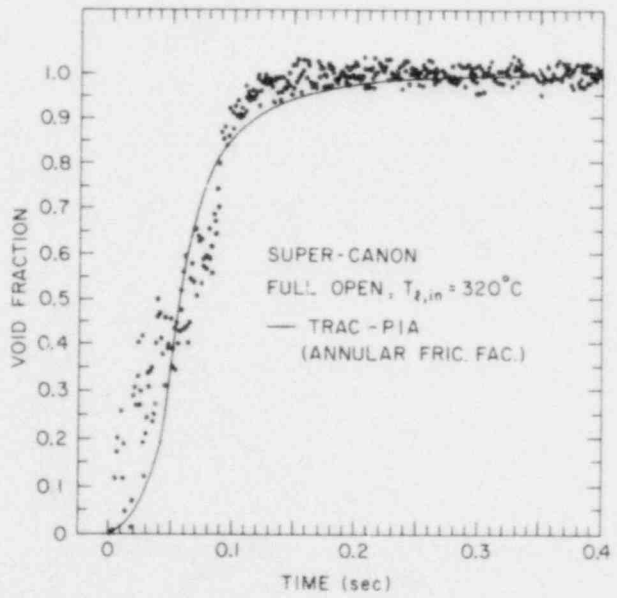

Fig. 4.16 Comparison of TRAC-PlA Prediction with the Void Fraction Data of the Super-CANON Test with Full Open Exit and $T_{\ell,in}$ = 320° C. (BNL Neg. No. 4-1331-80).

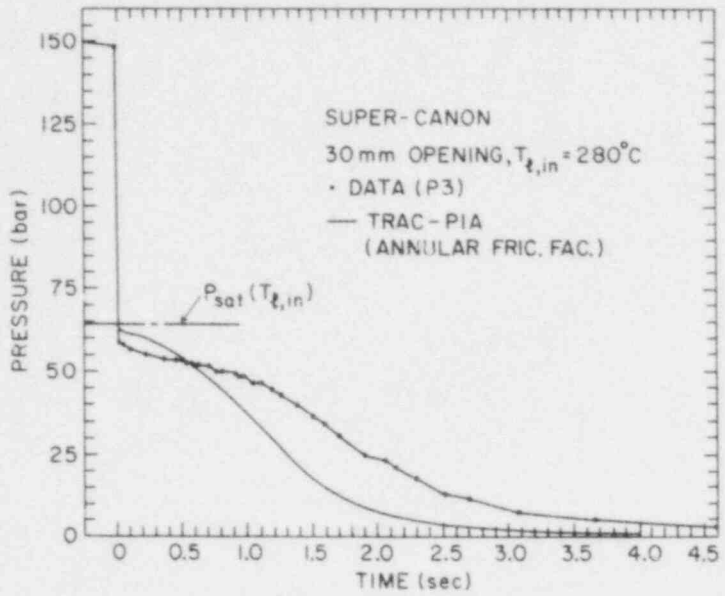

Fig. 4.17 Comparison of TRAC-P1A Prediction with the Pressure Trace of the Super-CANON Test with 30 mm Diameter Exit and $T_{\ell,in}$ = 280° C. (BNL Neg. No. 4-1330-80).

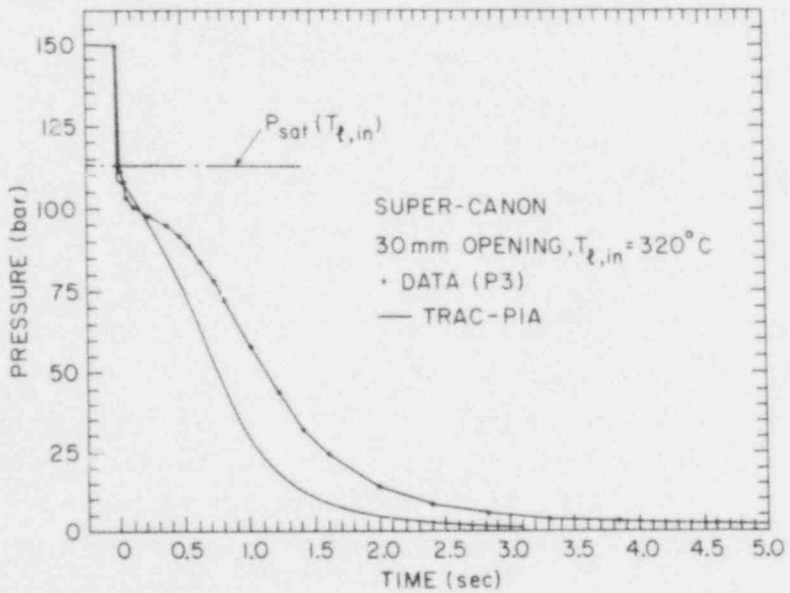

Fig. 4.18 Comparison of TRAC-P1A Prediction with the Pressure Trace of the Super-CANON Test with 30 mm Diameter Exit and $T_{\ell,in}$ = 320° C. (BNL Neg. No. 4-1329-80).

The first observation from the TRAC-P1A predictions for all these five tests is that the vessel top pressure is not predicted well for the first 1.5 seconds. In this time period the pressure in the vessel decreases rapidly, even below the saturation pressure and then recovers close to saturation pressure as the evaporation begins. This rapid drop in the vessel pressure in the beginning of the transient is due to subcooled blowdown and a delay in flashing in the vessel. The TRAC-P1A predictions do not show this dip in the vessel pressure because, in the code, the flashing begins as soon as the liquid becomes saturated. This early flashing also tends to keep the fluid closer to the equilibrium state and also explains why TRAC-P1A underpredicts the mass flow rate out of the nozzle for the first 10 to 20 seconds of the transient. The prediction is better for the case with minimum subcooling (7°C) and longest nozzle (L/D = 1.5) as expected (Test 20). Figures 4.19 and 4.20 show the plot of the ratio of computed and experimental vessel pressures as a function of time. Any departure from unity is an error in the prediction. The error in the early part of the transient is largest in Tests 22 and 24 as they have the largest subcooling. Figures 4.21 and 4.22 show the ratio of predicted and experimental mass flow rate at the nozzle. These curves have the same trend in error as the previous curves. Table 4.4 summarizes these observations for Tests 20 to 24. All of these tests except for Test 23 support the conclusion made here. Test 23 had some problem with the density measurement as all the three beams overpredicted the density. Two of these beams had overprediction in the first 10 and 20 seconds of the transient by 0-30 kg/m^3 and 0-70 kg/m^3, respectively. This explains the sudden rise in the mass flow rate at 5 seconds and large error in mass flux as shown in Table 4.4. Furthermore, the percentage error in the mass flux does not follow the same trend as the absolute error as they occur at different times in the transient.

Table 4.4 MARVIKEN CRITICAL FLOW TESTS 20, 21, 22, 23, 24 COMPARISON

Test	L/D	$(\Delta T)_{sub}$ °C	$(\Delta P)_{max}$ 0-10 sec bar	$(\Delta M)_{max}$ 0-20 sec kg/m^2s	Max % Error in P 0-10 sec	Max % Error in M 0-20 sec
20	1.5	7	2.0	-7500	4%	-25%
21	1.5	33	7.0	-8000	15.5%	-25%
22	1.5	52	8.0	-9000	15.5%	-20%
23	0.33	5	3.8	-22400	8%	-33%
24	0.33	33	8.4	-14000	19.5%	-34%

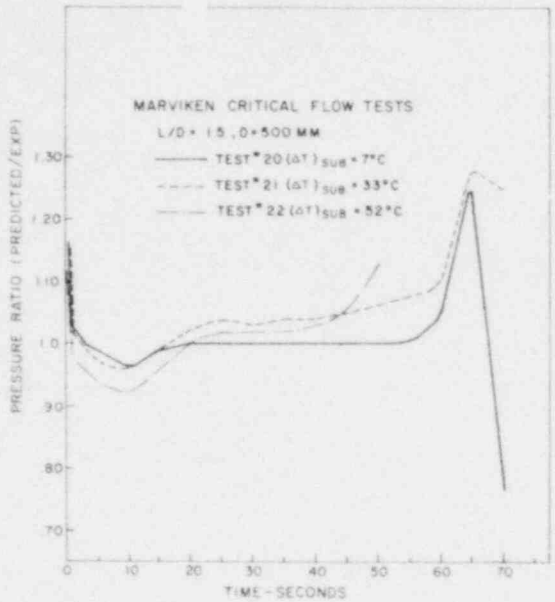

Fig. 4.19 The ratio of predicted and experimental values of the pressure at the top of the vessel as function of time for the Tests 20, 21, and 22. (BNL Neg. No. 5-335-80).

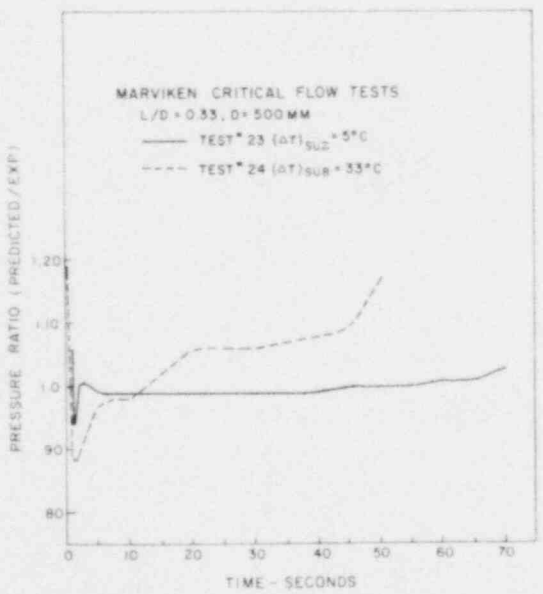

Fig. 4.20 The ratio of predicted and experimental values of the pressure at the top of the vessel as function of time for the Tests 23 and 24. (BNL Neg. No. 5-336-80).

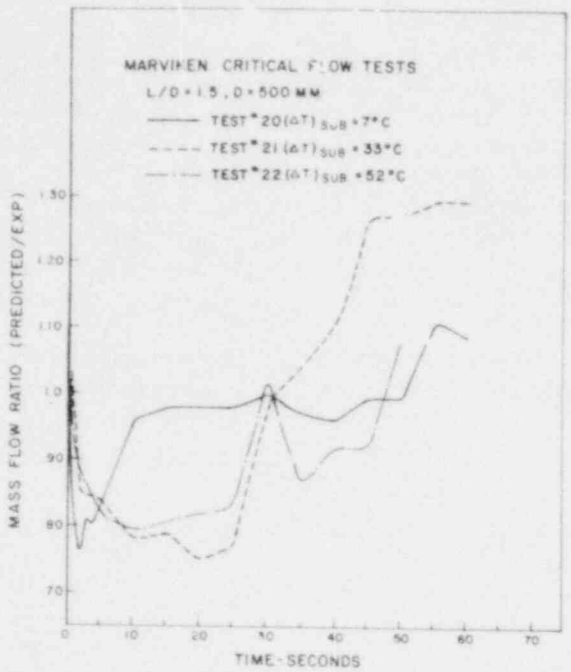

Fig. 4.21 The ratio of predicted and experimental mass flow rates as function of time for Tests 20, 21, and 22. (BNL Neg. No. 5-333-80).

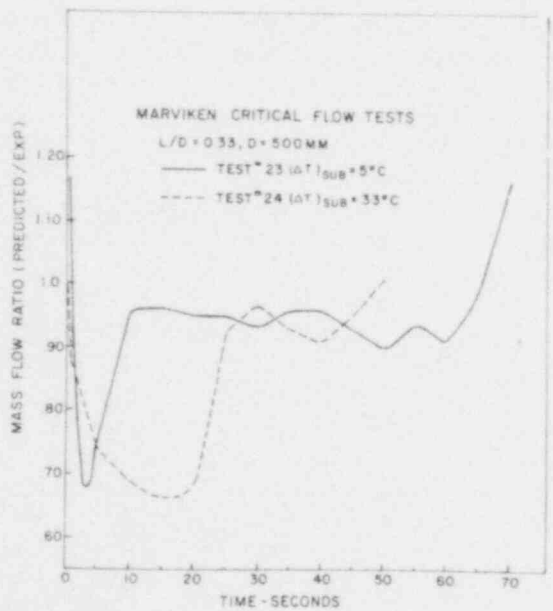

Fig. 4.22 The ratio of predicted and experimental mass flow rates as function of time for the Tests 23 and 24. (BNL Neg. No. 5-334-80).

4.6 Battelle-Frankfurt Top Blowdown Tests (L. Neymotin)

This experiment (Holzer, 1977) was carried out by Battelle-Institute in Frankfurt (Main), West Germany in 1977. It was a top blowdown test in a vessel of over 11m in height and 0.776m in diameter. A short discharge nozzle (D = 0.143m) was attached at about 1m from the top. Initially, the vessel was filled with subcooled water (p = 71 bar) at a temperature of 285°C up to 7m level. The vessel and the discharge nozzle were equipped with the instrumentation for measuring the temperature, pressure, mixture level in the vessel, void fraction and the mass flow rate in the nozzle during the first few seconds after the blowdown had begun. The data obtained should be useful for the TRAC code verifications.

At this point, the Battelle-Institute experimental data have been processed and a TRAC input deck has been prepared. Preliminary runs are currently being done.

4.7 RPI Phase Separation Tests (U.S. Rohatgi)

In the last quarter, the RPI Phase Separation Test 3 was attempted with and without mixing tee (Rohatgi, 1980b) and it failed to converge to steady state In this quarter, RPI Tests 1, 3, 6 and 8 were tried. This time mixing tee is modelled for all the tests so that the boundary conditions could be specified at the air and the water inlets, where the void fraction is correctly known. Tests 6 and 8 had 24 rods in the test section and the details are given elsewhere (Lahey, 1978). All of these tests were run and none of these converged to a steady state within a specified computer time limit of 500 seconds of CDC 7600. Tests 3 and 8 had both outlet pipes open and had symmetric initial and boundary conditions. Even though TRAC-P1A did not produce a converged steady state for these tests, the flow rate from the outlets did stabilize and the mass conservation was almost satisfied, as seen in Figures 4.23 and 4.24. However, the flow rate from the right hand side outlet was always greater than the left hand side outlet. Surprisingly, this difference was more in the case of Test 8 with the rods. The computation for Test 1 did not stabilize and the calculation stopped due to indefinite conditions reached in the program. The inlet and the outlet flow rates for this test are shown in Figure 4.25. Test 6 which had the rods and only one open outlet showed most promise even though TRAC-P1A did not converge to a steady state. Figure 4.26 shows the mass flow rate at the outlet and inlet for maximum time steps of 0.01 sec and 0.001 sec. Both the curves for the outlet flow rate seem to be converging to the inlet flow rate. The void fraction prediction for Test 6 in the lowest level and in the level near the outlet are compared with the data and are shown in Figure 4.27. As expected, there is an accumulation of air in the upper corner away from the exit. However, the experimental results show a decrease in the void fraction in the upper level which is in contradiction with physical expectation and TRAC-P1A predictions. The experimental results of Test 1 which is similar to Test 6 but without rods show higher void fraction in the level near the exit than near the inlet.

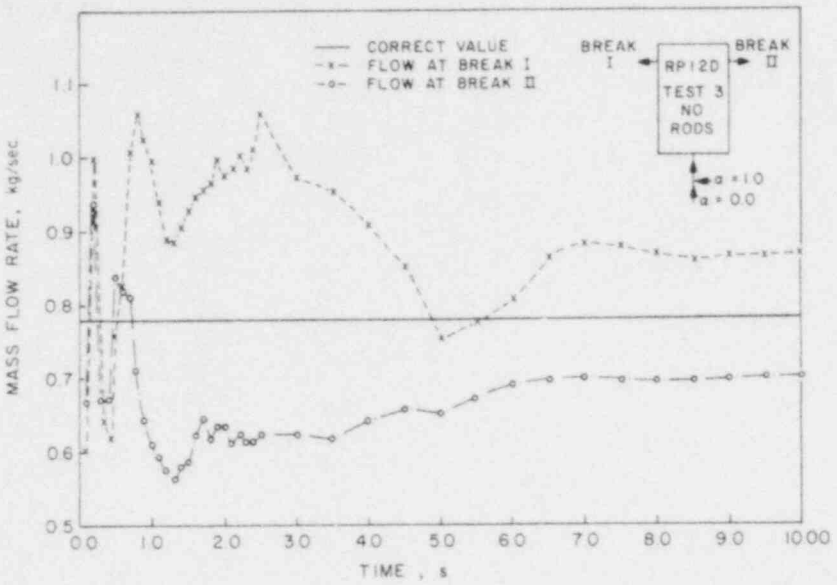

Fig. 4.23 TRAC-P1A Calculations for the RPI Test No. 3. (BNL Neg. No. 4-1344-80).

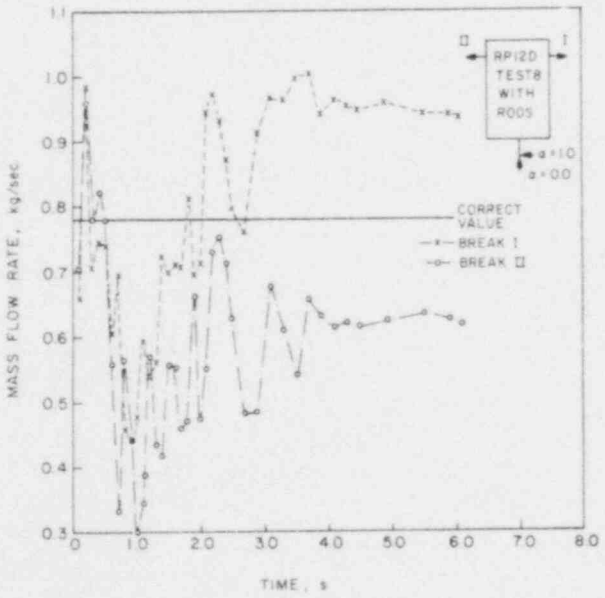

Fig. 4.24 TRAC-P1A Calculations for the RPI Test No. 8. (BNL Neg. No. 4-1343-80).

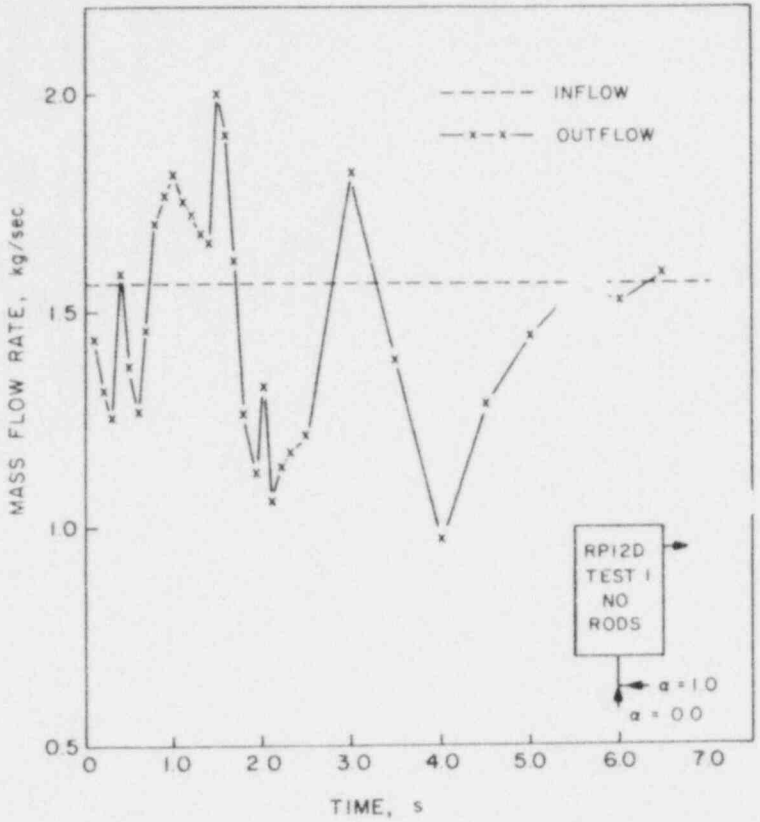

Fig. 4.25 TRAC-P1A Calculations for the RPI Test No. 1. (BNL Neg. No. 4-1320-80).

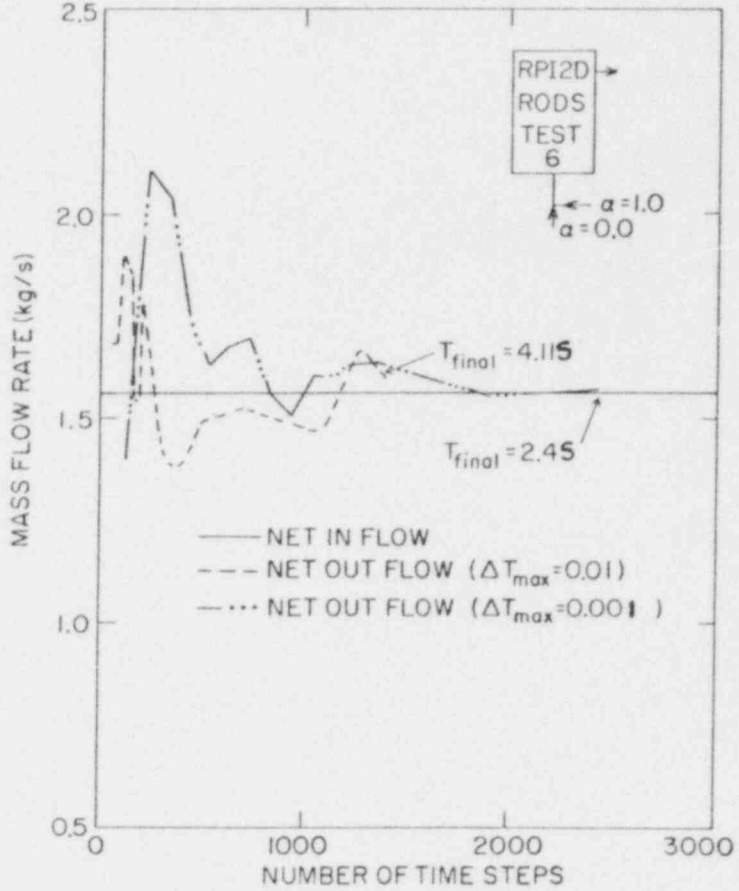

Fig. 4.26 TRAC-P1A Calculations for the RPI Test No. 6. (BNL Neg. No. 4-1317-80).

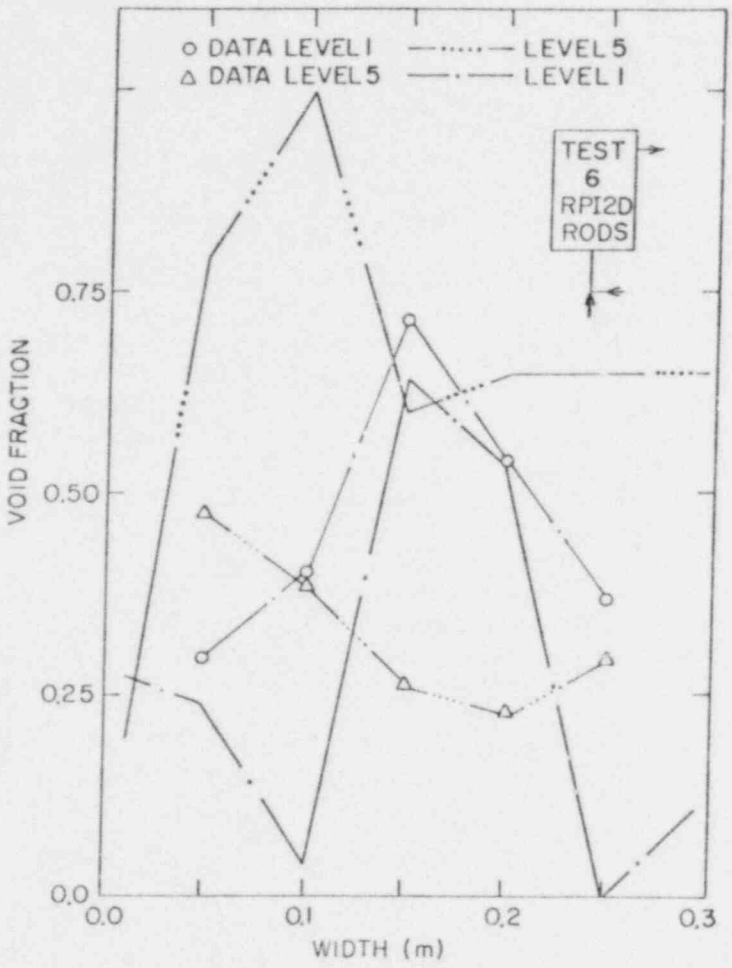

Fig. 4.27 Comparison of TRAC-P1A Prediction with the Void Fraction Data of RPI Test No. 6. (BNL Neg. No. 4-1319-80).

4.8 FRIGG-Loop Forced and Natural Circulation Tests (L. Neymotin)

After the 3-D FRIGG calculations had shown problems with reaching the steady-state, attention was concentrated on some issues which presumably could be responsible for the divergent results.

First, the effect of multidimensional hydrodynamics on the stability was checked. It was accomplished by switching to the 1-D vessel option provided by the TRAC. The calculations have been done and divergent results were obtained again (see Fig. 4.28). This suggests that the numerical instability in the vessel module may not be due to the multidimensional hydrodynamics, but probably due to some other reason. However, it is worthwhile to mention that the time averaged axial void distribution looked reasonable and could be compared with the experimental data. Figure 4.29 shows the experimental void distribution (1) being compared with the 1-D vessel computed result (2). The third curve in this figure represents the void distribution obtained by running the TRAC's PIPE component with the FRIGG's test conditions. In this run the convergence has been reached very quickly (apparently the drift-flux model used for the 1-D components has some numerical algorithm advantages over the two-fluid model employed in the vessel component that provide the drift-flux model with higher stability). Also, it is clearly seen from this figure to what extent the steady-state void distribution is affected by the absence of the subcooled boiling model in the TRAC-P1A.

The next attempt was made to see whether the two-fluid model works properly just for an adiabatic air-water flow in the 1-D FRIGG-like vessel. A few computer runs covering a wide range of inlet void fractions have been successfully performed. All of these runs converged to a steady-state rather quickly.

One more air-water run was performed (see Fig. 4.30) to make sure that the presence of a single phase two-phase boundary at some vessel level did not initiate the instabilities. Convergent results for this case were obtained without any problems.

Based on the results presented above, it may be concluded that the instabilities in the FRIGG-like tests are caused by the combination of the wall heating and vapor generation, strongly coupled with the two-fluid hydrodynamics.

4.9 Addition of Delayed Nucleation in TRAC-P1A (Y. Sanborn)

TRAC-P1A code modifications to include delayed nucleation in case of flashing for 1-D components were made using Alamgir-Lienhard criterion (1980) to calculate the underpressure, Δp_{Fio}, i.e., $p_{sat} - p_{nuc}$:

$$\Delta P_{Fio} = 0.258 \frac{\sigma^{3/2} \left(\frac{T_{in}}{T_c}\right)^{13.76} \left(1 + 13.25 \sum^{0.8}\right)^{0.5}}{\sqrt{K\, T_c} \left(1 - \frac{v_f}{v_g}\right)}$$

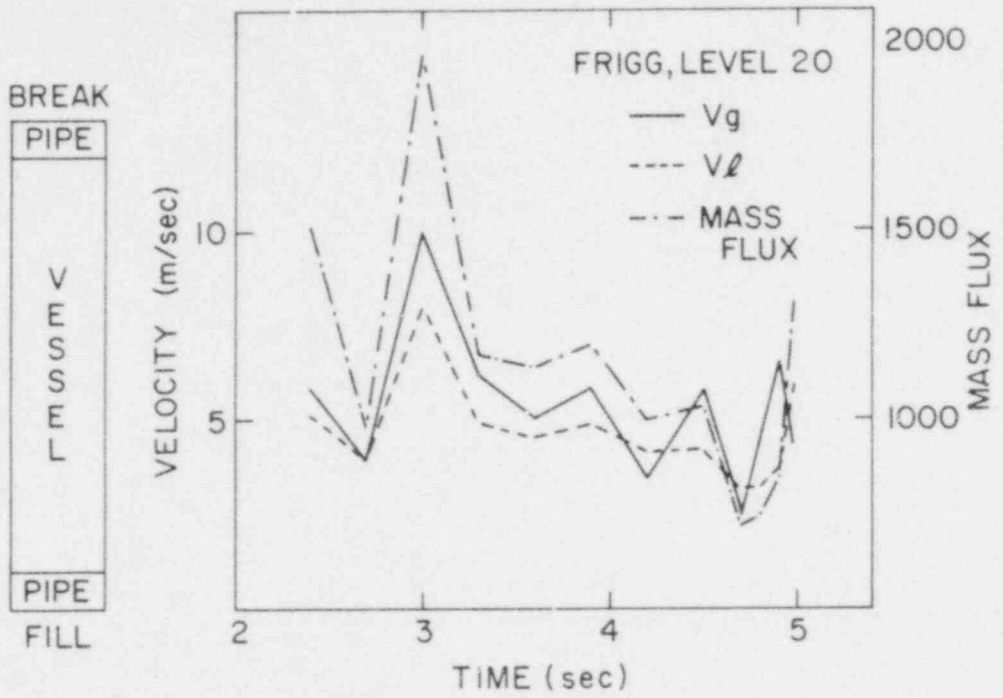

Fig. 4.28 Calculation of TRAC-P1A with 1-D Vessel Option for FRIGG test.

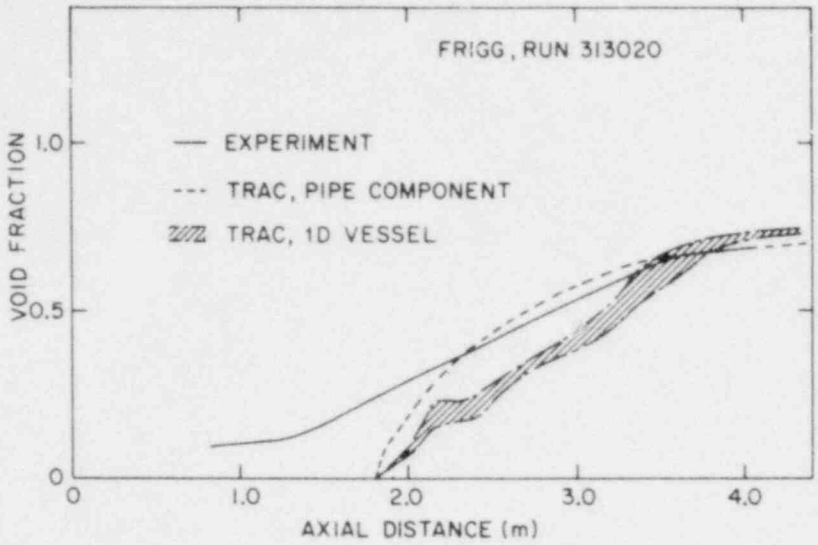

Fig. 4.29 Comparison of Various TRAC-P1A Calculations with the Void Fraction Data of the FRIGG Test. (BNL Neg. No. 5-332-80).

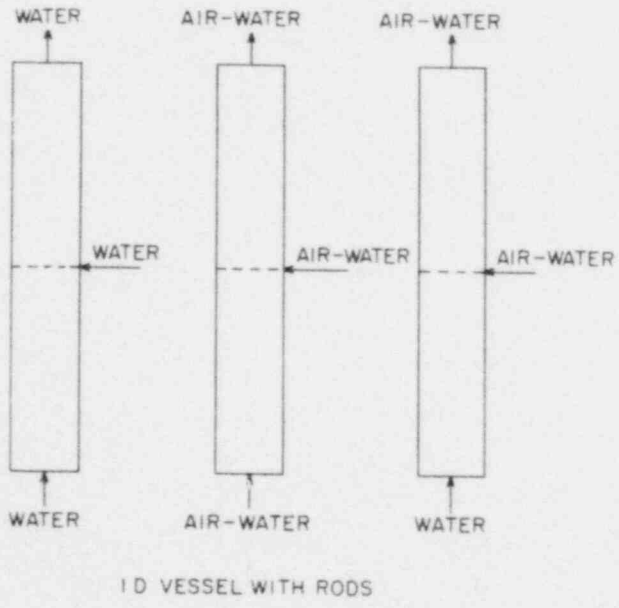

Fig. 4.30 Various Air-Water Test Configurations for TRAC-P1A Calculations with the 1-D Vessel Option. (BNL Neg. No. 4-1334-80).

where

σ = surface tension

T_{in} = inlet or initial liquid temperature

T_c = critical temperature

K = Boltzman's constant (1.38×10^{-23} J/K)

v_f = specific volume, liquid

v_g = specific volume, vapor

$\sum$ = depressurization rate in Matm/sec.

In order to implement the delayed nucleation, the variables ALV and CHTI which are the heat transfer rates per unit temperature difference to the interface from the liquid and from the vapor, respectively were set to zero in the interfacial heat transfer section of the constitutive package in subroutines DF1DS and DF1DI, unless the pressure dropped below the nucleation pressure, P_{nuc}, the donor cell is feeding voids, or some voids exist in the cell from the previous time step.

The BNL nozzle experiments are being simulated with this modification. Flashing in the pipe seems to start at the correct pressure, but steady-state solutions were not always attained. Some transient problems (e.g., Super-CANON tests) are being tried now.

REFERENCES

ALAMGIR, Md. and LIENHARD, J. H., (1980), "Correlation of Pressure Undershoot during Hot-Water Depressurization," to be published in the ASME Journal of Heat Transfer.

DUKLER, A. E. and SMITH, L. (1977), "Two Phase Interactions in Counter Current Flow: Studies of the Flooding Mechanism," NUREG-CR-0617, Annual Report November 1975 - October 1977.

ERICSON, L., et al (1979), "The Marviken Full Scale Critical Flow Tests", MXC-220, September 1979, Joint Reactor Safety Experiments in The Marviken Power Station, Sweden.

ERICSON, L., et al (1979), "The Marviken Full Scale Critical Flow Tests," MXC-221, September 1979, Joint Reactor Safety Experiments in the Marviken Power Station, Sweden.

ERICSON, L., et al (1979), "The Marviken Full Scale Critical Flow Tests," MXC-223, September 1979, Joint Reactor Safety Experiments in The Marviken Power Station, Sweden.

HOLZER, B., KANZLEITER, T., and STEINHOFF, F., "Determination of Water Level and Phase Separation Effects During the Initial Blowdown Phase," Battelle-Institute of Frankfurt (Main), February 1977.

ISHII, M., (1977), "One-Dimensional Drift-Flux Model and Constitutive Equations for Relative Motion Between Phases in Various Two-Phase Flow Regimes," ANL-77-47.

JEANDEY, C., and BARRIERE, G., (1979), "Partie I, Etude Experimentale d'Ecoulements Eau-Air a Grande Vitesse," DTCE/STT/SERTE Note T.T. No. 599, Janvier 1979.

KEDZIUR, F., (1978), "Investigation of Strongly Accelerated Two-Phase Flow," ICHMT Conf., Dubrovnik, Sept. 1978.

LAHEY, R. T., (1978), "Two-Phase Flow Phenomena in Nuclear Reactor Technology," Quarterly Progress Report 8, March-May, 1978, NUREG-CR-0418, 1978.

RIEGEL, B., (1979), "Experience Super-CANON," TT/SETRE/79-2-B/BR.

ROHATGI, U. S., (1980a), "Marviken Critical Flow Tests," in WRSRD Quarterly Progress Report, Reactor Safety Research Program, October-December 1979, BNL-NUREG-51178, April 1980.

ROHATGI, U. S., (1980b), "RPI Two Phase Separation Tests," in WRSRD Quarterly Progress Report, Reactor Safety Research Program, October-December 1979, BNL-NUREG-51178, April 1980.

SAHA, P., (1980), "Moby-Dick Nitrogen-Water Experiments," in WRSRD Quarterly Progress Report, Reactor Safety Research Program, October-December 1979, BNL-NUREG-51178, April 1980.

SRIKANTIAH, G., (1979), "KFK-IRE Nozzle Flow Tests," in WRSRD Quarterly Progress Report, Reactor Safety Research Program, April-June, 1979, BNL-NUREG-51081, NUREG/CR-1035, pp. 30-32.

II. METALLURGY AND MATERIALS EVALUATION

SUMMARY

The effects of service related variables on the stress corrosion cracking of Inconel 600 steam generator tubing are being determined experimentally and the data used to formulate a model for service life expectancy.

Several tests have been completed with fixed deflection specimens exposed to pure water, simulated primary or secondary (AVT) environments. Primary water appears to be slightly more aggressive in producing early failures.

Constant extension rate tests have been carried out to determine when crack initiation occurs in a slowly strained specimen. These results are being used to refine reported crack velocities calculated using the yield point of the material as the reference initiation point.

Inconel 600 capsule tests, used to provide a reverse denting type specimen, were terminated after 36 weeks. The slow deformation rates did not produce stress corrosion cracking.

1. Stress Corrosion Cracking of PWR Steam Generator Tubing

(T.S. Bulischeck and D. van Rooyen)

PWR steam generator tubing fabricated from Inconel Alloy 600 with processing histories typical of past and current production methods are being evaluated for stress corrosion cracking (SCC) susceptibility. A variety of test methods are being employed to study the effects of stress, strain, strain rate, environment and temperature on the failure times of the material. Data obtained from these experiments are being fitted to a model which can be used to predict the service life of steam generator tubing exposed to normal operating environments or adverse conditions such as denting.

Reverse tube U-bend spescimens are being used to determine the crack initiation times of highly stressed material such as may be expected for tubing which has dented, but the denting action has been arrested. Pure water exposures were conducted with duplicate specimens in the pickled and unpickled condition at test temperatures of 365°C, 345°C, 325°C and 290°C. The tests at the two highest temperatures were terminated after 36 weeks and the two lower temperature tests are continuing with several heats of material showing failures at 325°C at this time. Simulated primary water exposures at 365°C and 345°C and all volatile treatment (AVT) tests at 345°C and 325°C were scheduled to provide a two temperature comparison of the SCC susceptibility of Alloy 600 in three environments. The highest temperature tests for each of these service related environments have been completed and the lower temperature tests are continuing. Figures 1, 2, 3 show the time to failure versus temperature relationship for the five heats of mill annealed material which have exhibited intergranular SCC in the three test solutions. AVT exposures at 345°C produced faiure times very similar to those in pure water environments and well within the scatter band expected for a limited number of specimens. Figure 2 shows that primary water exposures at 365°C and 345°C for heats #10 (.0 C) and heat #11 (.0 C) produced failure times significantly lower but parallel to the pure water tests. The two low carbon heats (.01C) shown in Fig. 1 had varied responses to the primary water environment. Essentially, no difference in failure times existed for heat #4 in the two environments at 365°C but failure times were shorter in primary water at 345°C. None of the specimens from the other low carbon material (heat #5) cracked in primary water. The highest carbon heat #2 (.05C) in Fig. 3 again appears to fail more quickly in primary water at 345°C, but the results are reversed at 365°C. The general trend, therefore, shows primary water to be a slightly more aggressive environment than pure water.

Inconel 600 tubing processed with the current production methods i.e., a final heat treatment at 700°C for 20 hrs., was placed in both primary water and AVT environments. None of thee specimens have failed in the U-bend tests, however, material produced by the same manufacture and removed from line just prior to the thermal treatment has failed. This indicates that the final heat treatment and not any prior processing is very beneficial in preventing SCC in these environments.

1.1 Constant Extension Rate Tests (CERT)

The CERT test is being used to determine crack propagation rates by dividing the intergranular crack depth at failure by the exposure time from the yield point to the end of the test. This method assumed that the cracks initiated at the yield point, since data was not available to precisely determine the initiation point. Several tests have been carried out to determine this value. The specimens were strained at rates necessary to produce SCC, but were stopped at strain levels prior to total fracture and the crack depths measured. This data was extrapolated to zero crack depth to determine the initiation time. Figure 4 indicates that crack initiation in 365°C CERT occurs between the yield point and 2.2% strain past yield depending on how one elects to draw the line. In this case the data closest to the initiation point was weighted more heavily. The data in Figure 5 show the effect of recalculating the crack velocities using the newly determined initiation times in place of the yield point. The effect is small, but tends to bring the 365°C data more in line with the lower temperatures. Additional work will be done to determine the initiation point at the lower temperatures.

Tests are now in progress to obtain crack velocities for specimens without any cold work, since those used for the majority of the tests have a small amount due to flattening the tubing material into plate type tensile specimens.

1.2 Cyclic Stress Tests

Cyclic stress tests are continuing with the strain rate of the specimen being recorded throughout the test and an effort is being made to correlate these results with the data received from other test methods.

1.3 Constant Stress Tests

Tests have been completed for one low carbon heat of material and these results indicate that the failure time is proportional to σ^{-3}. The higher carbon material (heat #2) which is currently in test is requiring a much longer time to produce SCC.

1.4 Capsule Tests

Inconel 600 capsules with a corroding carbon steel slug inside and primary water outside were being used to explore the effects of slow deformation rates and complex stress patterns on crack initiation. These capsules were bulged by the corrosion products so that 20 mils of diametral deformation occurred during 35 weeks of exposure. These tests have been terminated since the very slow deformation rates did not produce SCC.

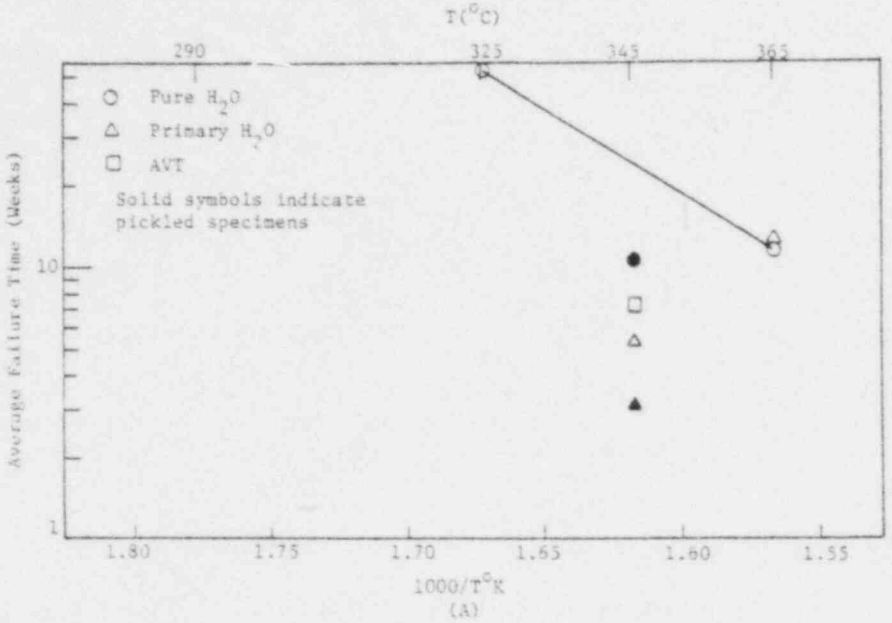

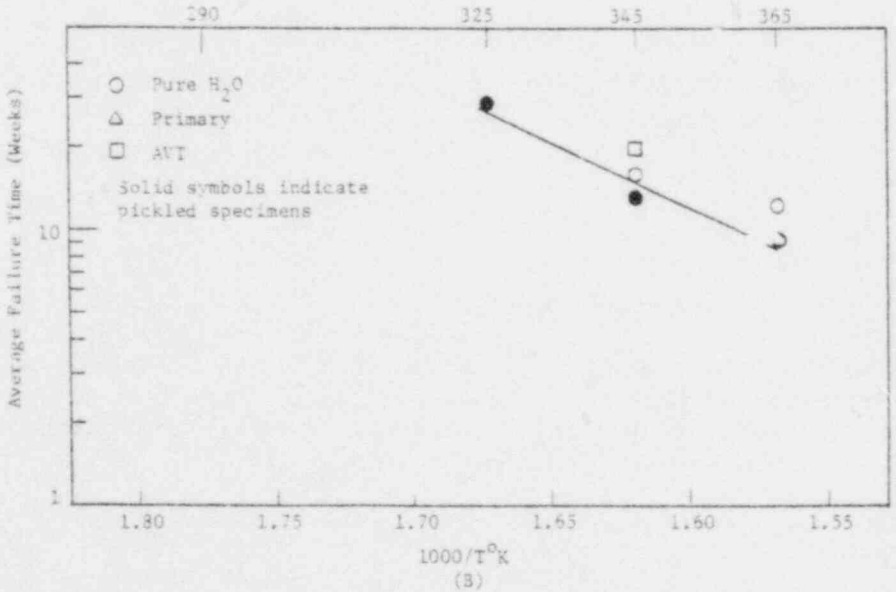

Fig.1 Effect of environment, surface preparation and temperature on failure time of U-bend specimens (A) Heat #4 (B) Heat #5

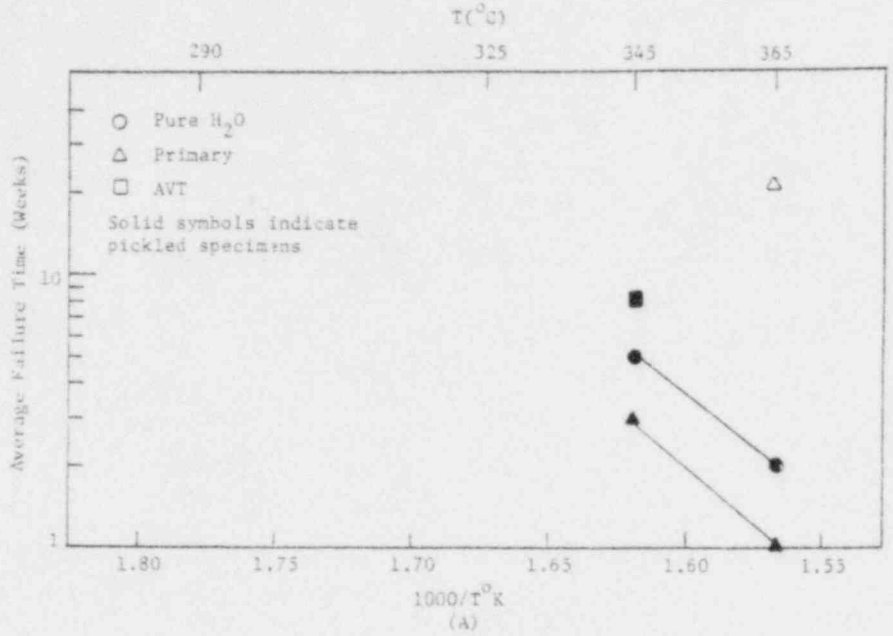

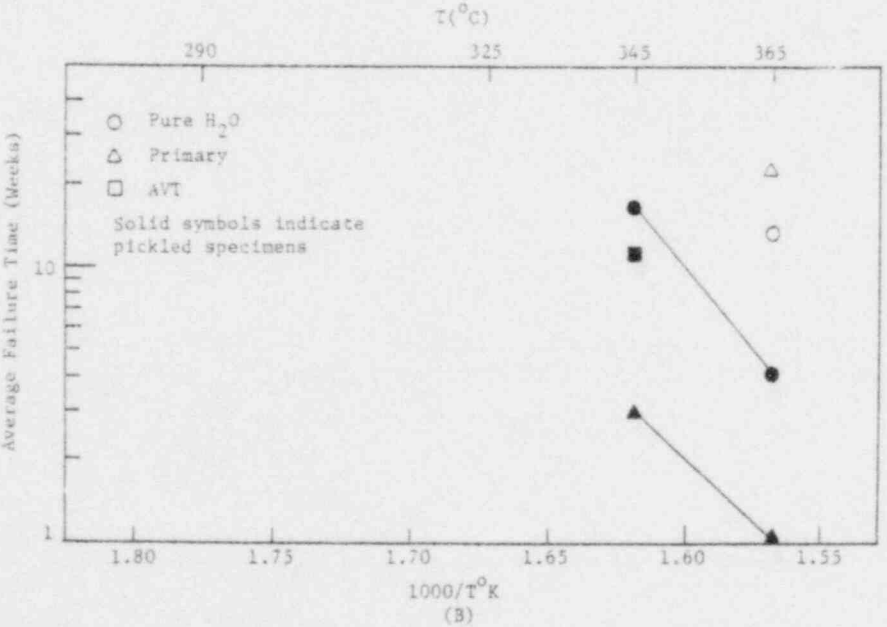

Fig.2 Effect of environment, surface preparation and temperature on failure time of U-bend specimens (A) Heat #10 (B) Heat #11

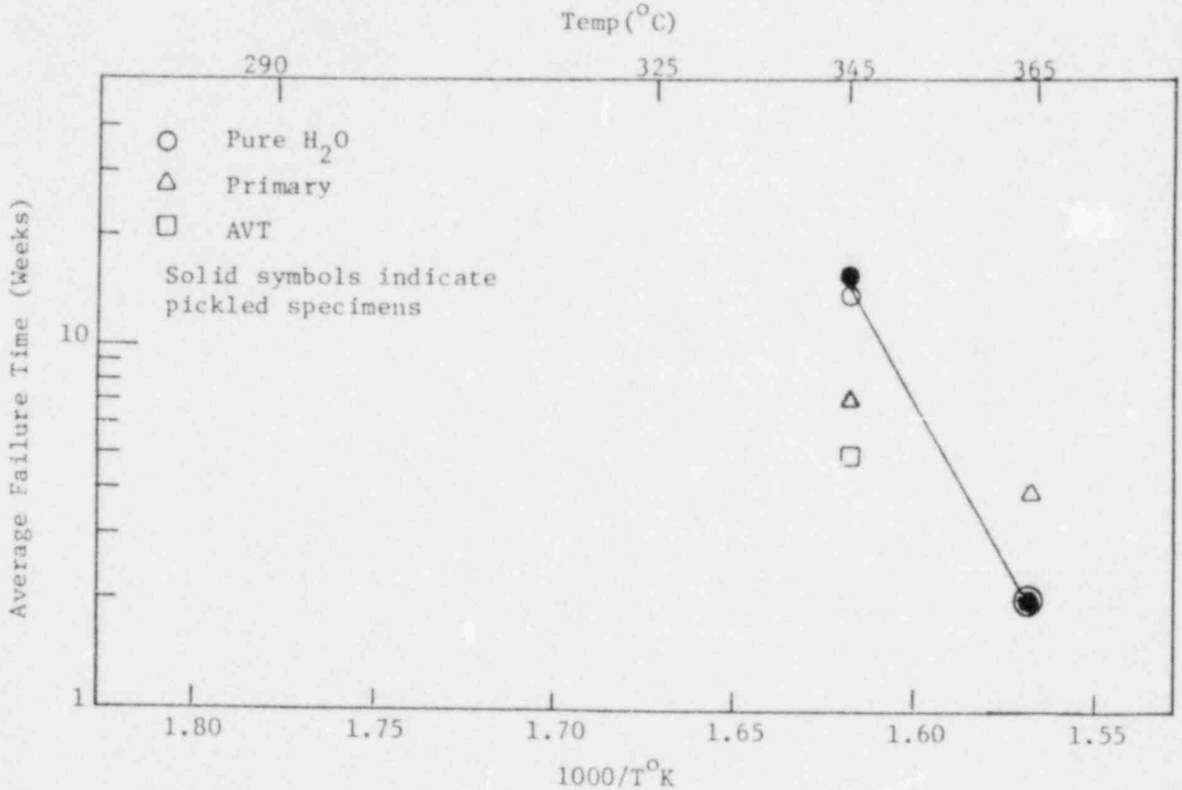

Fig. 3 Effect of environment, surface preparation and temperature on failure time of U-bend specimens Heat #2

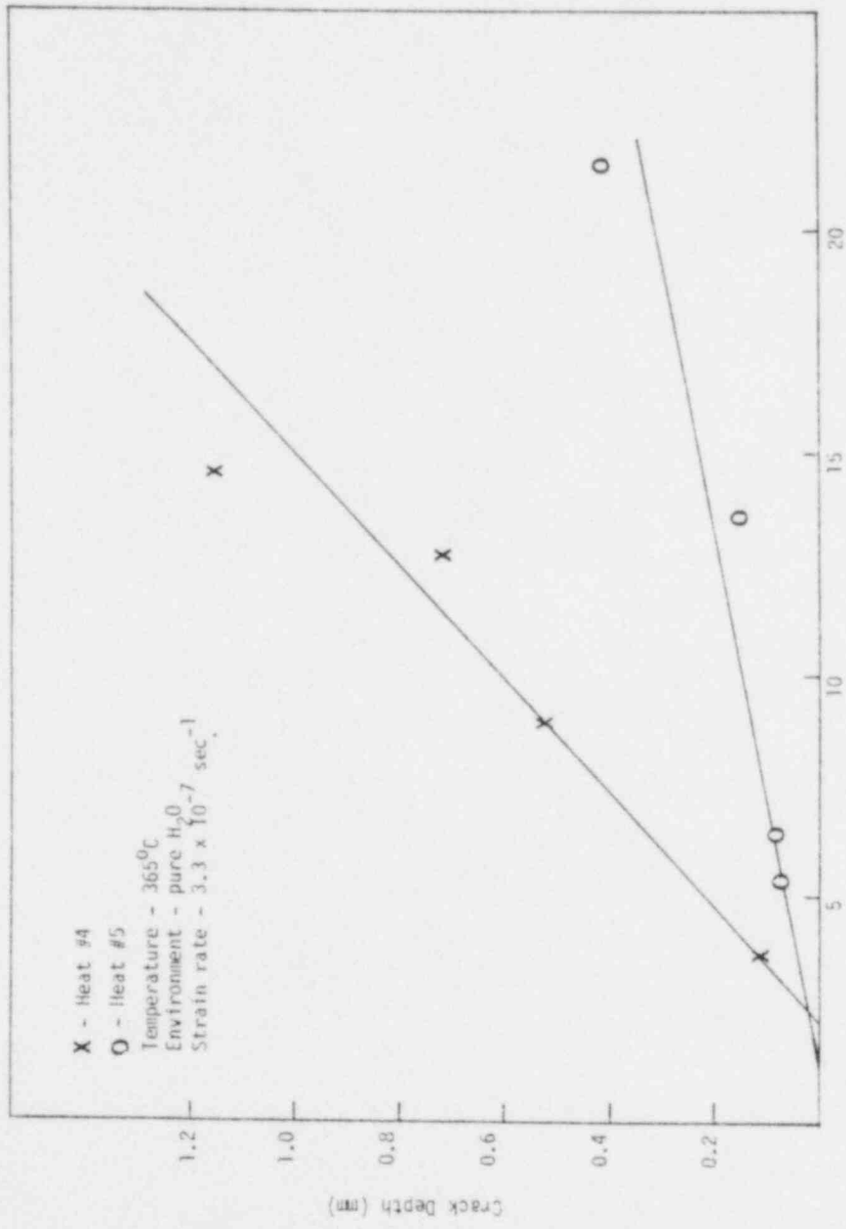

Fig. 4 Determination of Crack Initiation in 365°C CLRT Exposure

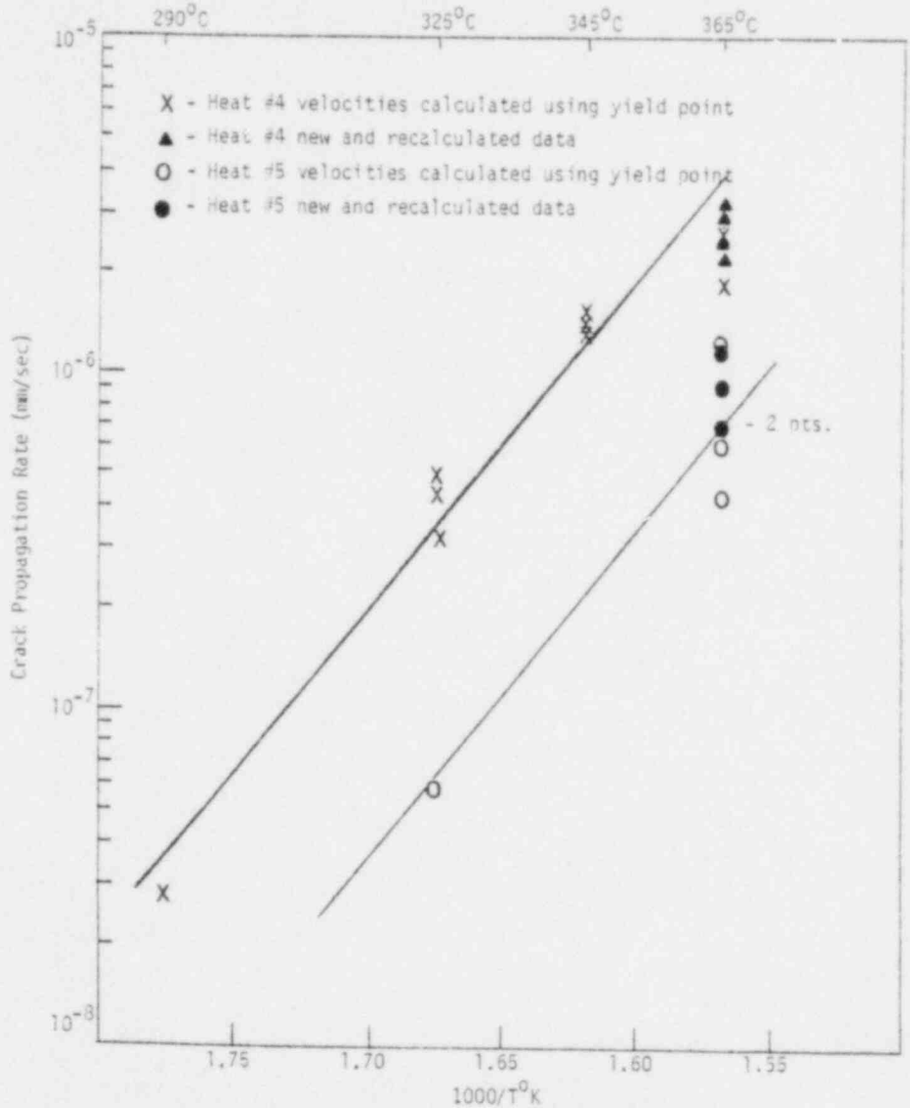

Fig. 5 Charge in previously reported data after determining crack initiation in 365°C slow strain rate tests